How does stiffness of polymer chains affect their adsorption transition?

A. Milchev[1], Binder[2]
[1] *Institute of Physical Chemistry, Bulgarian Academy of Sciences, 1113 Sofia, Bulgaria [milchev@ipc.bas.bg] and*
[2] *Institut für Physik, Johannes Gutenberg-Universität Mainz,*
Staudinger Weg 9, D-55099 Mainz, Germany [kurt.binder@uni-mainz.de]

The adsorption transition and the structure of semiflexible adsorbed macromolecules is studied by Molecular Dynamics simulation of a coarse-grained bead-spring type model. Varying chain length N and stiffness κ (which is proportional to the persistence length ℓ_p in $d = 3$ dimensions) as well as the strength ϵ_{wall} of the adsorption potential, the adsorbed monomer fraction, orientational bond order parameter, and chain linear dimensions are studied. In the simulations excluded volume interactions normally are included but can be "switched off", and thus the influence of excluded volume (leading to deviations from predictions of the wormlike chain model) can be identified. It is shown that the variation of the adsorption threshold ϵ^{cr}_{wall} with ℓ_p is compatible with the predicted law $\epsilon^{cr}_{wall} \propto \ell_p^{-1/3}$. Near the transition the decay length of orientational correlations along the chain contour increases gradually from ℓ_p to $2\ell_p$. While the latter value is expected for strictly two-dimensional chains from the Kratky-Porod model, this model is inaccurate for the description of lateral chain dimensions of long strongly adsorbed semiflexible polymers due to its neglect of excluded volume. The significance of these findings for the interpretation of pertinent experiments is briefly discussed.

I. INTRODUCTION

Adsorbed polymers on surfaces are of great interest for applications in materials science and in biological context, and find extensive attention since decades [1–5]. For instance, DNA oligonucleotides adsorbed on graphene and graphene oxide are of interest also for applications for new sensors and related devices [6]. Already the conceptually simplest case, adsorption of fully flexible linear chain-like neutral macromolecules, has turned out to be a challenging problem of statistical thermodynamics, due to the interplay between surface-monomer and monomer-monomer forces with the configurational entropy of the polymers [7–15]. However, for many real polymers the effect of their bending rigidity matters, causing nontrivial bond-angle correlations over the scale of the persistence length [16–19]. While for simple synthetic polymers such as polyethylene or polystyrene the persistence length ℓ_p is only of the order $1nm$, i.e., a few bond lengths ℓ_b along the chain backbone, more complex synthetic polymers exhibit significantly larger [18] ℓ_p. Particularly important is this local chain stiffness for many biopolymers, e.g. double-stranded (ds) DNA, filamentous (F)-actin, microtubules, etc. For ds-DNA ℓ_p is roughly $50nm$, and the effective diameter of this molecule (which in a coarse-grained view is locally rod-like) is about [20] $D = 2nm$ (but note that DNA carries electric charges, and it may be better to use an effective diameter depending on the salt concentration in the solution [21]). For F-actin, typical [22] values are $\ell_p = 17\mu m$, $D \approx 8nm$, and contour lengths can be of the order of $L = 10\mu m$: note that the mechanical rigidity of these molecules is often crucial for their biological function, e.g., actin filaments form the cytoskeleton of cells, and adsorption of actin or DNA on membranes has been widely studied [22–26]. Of course, also adsorption of these molecules on various inorganic substrates (glass surfaces, graphite, mica, etc) is of interest [27–32] in the context of atomic force microscopy (AFM) measurements on these polymers. Particularly intricate is the problem of adsorption of polymers with more complex architecture, such as bottlebrush polymers [33–36] or dendronized polymers [37].

Varying grafting density and/or chain length of the side chains of bottlebrushes, their persistence length (together with their effective diameter) can be varied [38], but understanding this variation is difficult [19, 35, 39]. Likewise, the persistence length and effective diameter of dendronized polymers depends on their generation number, but again understanding this dependence is a challenge [40–43]. These problems are no surprise, since even for stiff polymers with much simpler chemical architecture estimates for ℓ_p from complementary methods often differ by as much as a factor of two [18]. When

adsorbed semiflexible polymers are studied with the intention to understand their persistence length in bulk solution [27–34, 37], clearly the effect of adsorption on the conformation of semiflexible polymers needs to be understood, and clarifying this problem is one aim of the present paper.

For flexible linear polymers, the adsorption transition has been described as a critical phenomenon in the framework of renormalization group theory [2, 12], i.e. various properties in the immediate vicinity of the transition (which is a sharp transition only in the limit where the chain length $N \to \infty$) are characterized by singular behavior involving universal critical exponents. However, for a full description of the transition (including how its location depends on the nature of the substrate-monomer interaction, non-universal prefactors of the various singular quantities, etc.) extensive numerical simulations (e.g. [12–15]) are required. A popular choice for this purpose in the case of flexible polymers is the self-avoiding walk (SAW) on a lattice [44]. For an extremely short-range adsorption potential (acting only on monomers in the first lattice plane adjacent to the substrate) of strength $\epsilon_{\rm wall}$, it is clear that the adsorption transition occurs when the entropy per monomer (of order k_BT) is of the same order of magnitude.

If one extends such a lattice model to semiflexible polymers by introducing an energy cost ϵ_b when two subsequent bonds along the chain form on angle [45–47], for $\epsilon_b \gg k_BT$ a chain conformation, roughly speaking, is a sequence of straight pieces of the order of the persistence length ($\ell_p \propto \exp(\epsilon_b/k_BT)$ in this limit. When such a piece is bound to the substrate, an energy of order $\ell_p\epsilon_{\rm wall}$ is won, while the entropy loss still is only of order k_BT. Thus, the critical temperature T_c of the adsorption transition scales as [45–47] $\epsilon_{\rm wall}/k_BT_c \propto \ell_b/\ell_p$.

While such a model may provide a qualitatively realistic description of chain stiffness for alkane-like polymers [48], where it is a good approximation to treat the bond angle of two successive carbon-carbon bonds as a discrete variable (controlled by the torsional potential [49]), it is not appropriate for biopolymers such as DNA, F-actin etc., where on the scale of ℓ_p a large number of C-C-bonds contribute, and chain bending occurs essentially continuously due to many small increments per covalent bond [48].

This situation is traditionally modelled by the Kratky-Porod (KP) wormlike chain (WLC) model [50], where a single energetic parameter (the bending stiffness κ) controls the polymer conformation locally, with $\ell_p \propto \kappa$. For the adsorption of WLCs a very different scaling of the adsorption transition temperatures with stiffness is predicted, namely [51–53] $\epsilon_{\rm wall}/k_BT_c \propto \ell_b/(\Delta^2\ell_p)^{1/3}$, provided the range Δ of the adsorption potential is small, $\Delta \ll \ell_p$. Only for the (unphysical) case of a square-well adsorption potential of range $\Delta > \ell_p$ a different law is predicted [53], $\epsilon_{\rm wall}/k_BT_c \propto \ell_b\ell_p/\Delta^2$.

The different scaling of WLCs and semiflexible chains on lattices can be qualitatively understood invoking Odijk's [54] deflection length concept. While on the lattice a piece of the chain, when it wins an energy $\epsilon_{\rm wall}$ per monomer, must be strictly parallel to the surface, this is not true for a KP chain. In fact, when a piece of a chain is confined within the range Δ close to the surface, one can show that typical conformations resemble straight pieces of length λ misaligned by an angle of order Δ/λ relative to the surface. The KP model yields [54] the deflection length λ as $(\Delta^2\ell_p)^{1/3}$, and the adsorption transition occurs when the energy won by the adsorption of the number of monomers $n_d = \lambda/\ell_p$ belonging to the deflection length is of order k_BT, i.e., $\epsilon_{\rm wall}(\Delta^2\ell_p)^{1/3}/\ell_b = k_BT$.

However, the KP model completely neglects excluded volume interaction between the monomers, and while in $d = 3$ dimensions for large ℓ_p and not too large contour length L ($L/\ell_b \ll (\ell_p/\ell_b)^3$) this is a good approximation [55–57] it clearly fails in $d = 2$, since topology forbids chain intersection strictly. Simulations [58–60] show that near $L/\ell_p = 1$ a smooth crossover occurs from rod-like behavior (mean square end-to-end distance $\langle R^2\rangle \approx L^2$ for $L < \ell_p$) to self-avoiding walk behavior ($\langle R^2\rangle \propto L^{3/2}\ell_p^{1/2}$ for $L \gg \ell_p$; note that the Flory exponent $\nu = 3/4$ in $d = 2$ dimensions [61]) rather than the Gaussian chain behavior [16, 17] $\langle R^2\rangle = 2L\ell_p$ implied by the KP model. E.g., for $L = 20\ell_p$ the KP model underestimates $\langle R^2\rangle$ by about a factor of two. Near the adsorption transition,

chain conformations change continuously from three-dimensional to two-dimensional, and hence it is relevant to clarify the extent to which excluded volume effects are important here.

Another intriguing problem is the fact that the effective persistence length, that controls the exponential decay predicted for the tangent-tangent correlation function with the distance along the chain backbone, is $\ell_p = \kappa/k_BT$ in $d = 3$, according to the KP-model, but $2\kappa/k_BT$ in $d = 2$. This doubling of the decay length occurs because in $d = 2$ there is only one direction transverse to the chain backbone, while in $d = 3$ there are two directions. A chain near the adsorption transition, however, is somewhat "in between" the dimensionalities (Fig. 1): Parts of the chain exist then in sequences of monomers that are adsorbed already (the so-called "trains" [1]), other monomers belong to "loops" and "tails" that extend out into the $d = 3$ space. Thus, it needs to be clarified what the concept of a persistence length means for such an incompletely adsorbed polymer chain. This is also an issue that we wish to clarify in the present study.

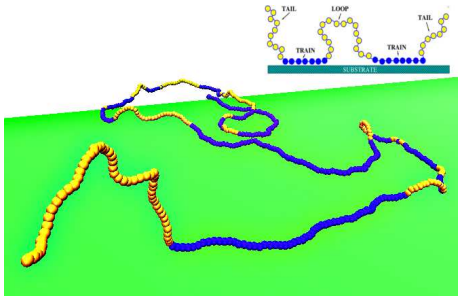

FIG. 1: Snapshot picture of an adsorbed chain with $N = 500$ monomeric units for the choice of parameters $k_BT = 1$, $\kappa = 16$, $\epsilon_{\rm wall} = 0.65$. The monomers are depicted as spheres of diameter $\sigma = \ell_b = 1$, and are shown in dark blue color when they belong to trains, and in yellow when they belong to loops or the tail. The chain is grafted by one end at the surface (green-shaded). In the upper part, a qualitative sketch explaining the notion of tails, trains and loops is given. For the simulated model shown here, the adsorption transition occurs at $\epsilon_{wall}^{cr} \approx 0.53$, so the shown state is about 20% off the transition into adsorbed phase.

The outline of our paper is as follows: in Sec. II, we summarize the pertinent theoretical background. In Sec. III, the model and simulation technique are briefly described. Sec. IV describes our methods to locate the critical value $\epsilon_{\rm wall}^{\rm cr}/k_BT$ (varying $\epsilon_{\rm wall}$ at fixed T, rather than varying T at fixed adsorption energy) where the adsorption transition occurs. The adsorption of fully flexible chains is also briefly considered as a special case. Sec. V describes the properties of adsorbed chains. Finally, Sec. VI summarizes our conclusions. A preliminary account of our result was given elsewhere [62].

II. POLYMER ADSORPTION: THEORETICAL BACKGROUND

For flexible polymers, polymer adsorption is a continuous transition [2] for which very close to the transition a scaling description applies. When the chain length N tends to infinity, and the relative distance from the adsorption threshold $\tau \equiv (\epsilon_{\rm wall} - \epsilon_{\rm wall}^{\rm cr})/\epsilon_{\rm wall}^{\rm cr}$ tends to zero, quantities like the components of the mean square end-to-end distance $\langle R^2 \rangle$ and gyration radius $\langle R_g^2 \rangle$ parallel ($||$) and perpendicular ($\perp$) to the surface, or the fraction of monomers f that are within the range Δ of the adsorption potential, do not depend on the two parameters N, τ separately, but in scaled form [12]

$$\langle R_g^2 \rangle_{||} = N^{2\nu} F_{||}(\tau N^{\varphi}) \, , \, \langle R_g^2 \rangle_{\perp} = N^{2\nu} F_{\perp}(\tau N^{\varphi}) \tag{1}$$

where ν is the Flory exponent [61] in $d = 3$, $\nu \approx 0.588$, and φ is the so-called *crossover exponent*. The precise value of this exponent has been controversial for decades [2, 9, 12–15], the most recent (and presumably accurate) value being [15] $\varphi \approx 0.48$. The scaling functions $F_{||}(X)$, $F_{\perp}(X)$ vary

with the scaling variable $X = \tau N^{\varphi}$ as follows,

$$F_{||}(X \to -\infty) = C_{||}^{-}, \quad F_{||}(X = 0) = C_{||}^{0}, \quad F_{||}(X \to +\infty) \propto |X|^{2(\nu_2 - \nu)/\varphi} \tag{2}$$

where $\nu_2 = 3/4$ is the Flory exponent in $d = 2$. Similarly,

$$F_{\perp}(X \to -\infty) = C_{\perp}^{-}, \quad F_{\perp}(X = 0) = C_{\perp}^{0}, \quad F_{\perp}(X \to +\infty) \propto |X|^{-2\nu/\varphi}; \tag{3}$$

Of course, the last of these relations implies that $\langle R_g^2 \rangle_{\perp}$ becomes independent of N in the strongly adsorbed phase,

$$\langle R_g^2 \rangle_{\perp} \propto \tau^{-2\nu/\varphi}, \tau N^{\varphi} \gg 1, \tag{4}$$

so $(\langle R_g^2 \rangle_{\perp})^{1/2}$ measures the thickness of the adsorbed ("pancake"-like) polymer coil. The constants $C_{||}^{-}, C_{||}^{0}, C_{\perp}^{-}, C_{\perp}^{0}$ in Eqs.(2,3) need not be further discussed here.

Finally,

$$f = N^{\varphi - 1} \tilde{f}(X) \tag{5}$$

with

$$\tilde{f}(X \to -\infty) \propto X^{-1} \quad , \quad \tilde{f}(0) = \text{const}, \quad \tilde{f}(X \to +\infty) \propto X^{(1-\varphi)/\varphi} \tag{6}$$

In the nonadsorbed phase, the adsorbed fraction (of order $1/N$) is just an effect due to the grafted chain end, while in the adsorbed phase $f \propto \tau^{(1-\varphi)/\varphi} \approx \tau^{1.08}$ can be considered as an order parameter of the transition. Note that for Gaussian chains the same scaling description applies, but then $\nu_2 = \nu = 1/2$ and $\varphi = 1/2$, so $f \propto \tau$ and $F_{||}(X \to +\infty)$ tends to a constant. Testing for the attraction strength ϵ_{wall} of the adsorbing surface for which a power law decay $f \propto N^{-(1-\varphi)}$ occurs is traditionally used as a criterion to locate $\epsilon_{\text{wall}}^{\text{cr}}$; this asymptotic power law is only seen for very large N, however [15].

The above scaling description can be taken as a justification of another method to locate $\epsilon_{\text{wall}}^{\text{cr}}$, namely the search for an intersection point of the ratio $\langle R_g^2 \rangle_{\perp} / \langle R_g^2 \rangle_{||}$ which is a dimensionless quantity and a function of τN^{φ} only, when corrections to scaling can be neglected. I.e.

$$\langle R_g^2 \rangle_{\perp} / \langle R_g^2 \rangle_{||} = F(\tau N^{\varphi}) \tag{7}$$

with

$$F(X \to -\infty) = C_{\perp}^{-}/C_{||}^{-} \, , \, F(X = 0) = C_{\perp}^{0}/C_{||}^{0} \, , \, F(X \to +\infty) \propto |X|^{-2\nu_2/\varphi}. \tag{8}$$

The scaling function $F(X)$ is universal, apart from a scale factor of its argument. The universal number $F(X = 0)$ has been estimated as [15] ($F(X = 0) = 0.320 \pm 0.003$; however, for the lattice model considered in [15] chain lengths N of the order of $N = 10^4$ were needed to obtain a reliable estimate.

In the theory summarized so far, stiffness does not play any explicit role; it would only show up in the (nonuniversal) prefactor of quantities such as the gyration radius square in the bulk $\langle R_g^2 \rangle_{\text{bulk}}$ (and similarly then in $\langle R_g^2 \rangle_{||}$, $\langle R_g^2 \rangle_{\perp}$ for chains grafted to a surface). However, for large stiffness this asymptotic scaling regime is only reached for extremely large N, hardly of physical interest. Therefore, it is necessary to analyse this pre-asymptotic regime that occurs for semiflexible polymers in its own right.

It is useful to describe a semiflexible polymer in terms of three lengths: its contour length L, its persistence length ℓ_p, and its effective diameter D. In terms of a model using effective monomers of spherical shape, such that subsequent monomers touch each other, the bond length $\ell_b = D$ and $L = (N-1)\ell_b$). In terms of the variable $n_p = L/\ell_p$, there occur then three regimes for the mean square end-to-end distance $\langle R^2 \rangle$, in $d = 3$ dimensions [55–57], namely, a rod-like regime, Random Walks (RWs), and Self-Avoiding random Walks (SAWs) regimes:

$$\textbf{Rods}: \langle R^2 \rangle = L^2, n_p \ll 1; \textbf{RWs}: \langle R^2 \rangle = 2\ell_p L,\ 1 \ll n \ll n_p^*; \textbf{SAWs}: \langle R^2 \rangle \propto 2\ell_p^2 \Big(\frac{\ell_p}{D}\Big)^{-2/5} n_p^{6/5}, n \gg n_p^* \tag{9}$$

where $n_p^* = (\ell_p/D)^2$, and the Flory approximation $\nu = 3/5$ was used.

While the Kratky-Porod model [50] describes the (smooth) crossover at $n_p = 1$ explicitly, the second crossover at $n_p = n_p^*$ relies only on crude scaling arguments, within the spirit of Flory's treatment of excluded volume [55]. Numerical work [57] is in rough argument with this description. In $d = 2$ dimensions, however, the intermediate gaussian regime is absent, and a single crossover from rod-like behavior to self- avoiding walk behavior occurs [58–60]

$$\langle R^2 \rangle = L^2, n_p \ll 1; \langle R^2 \rangle \propto \ell_p^{1/2} L^{2\nu_2} = \ell_p^{1/2} L^{3/2}, \quad n_p \gg 1. \tag{10}$$

We now summarize the predictions of the Kratky-Porod model in more detail. The wormlike chain is described by a curve $\vec{r}(s)$ in continuous space, with $0 < s < L$ a coordinate along this curve. The Hamiltonian of the chain is then an integral over the squared curvature along the curve,

$$\mathcal{H} = \frac{\kappa}{2} \int_0^L ds \Big(\frac{d^2\vec{r}(s)}{ds^2}\Big)^2. \tag{11}$$

The tangent-tangent correlation function

$$C(s - s') = \langle \cos\theta(s - s') \rangle \quad , \tag{12}$$

$\theta(s)$ being the angle between the tangent to the curve at site s, can be shown to be a simple exponential,

$$C(s) = \exp(-s/\ell_p), \quad \ell_p = \kappa/k_B T, \tag{13}$$

with k_B being Boltzmann's constant and T the absolute temperature. Eq. (13) refers to $d = 3$ dimensions, where two transverse directions exist relative to the tangent of the curve in each point. In $d = 2$ dimensions, where only a single transverse direction occurs, the decay of $C(s)$ is also exponential, but the decay length is twice as large

$$C(s) = \exp(-s/2\ell_p)\ , d = 2. \tag{14}$$

Note that Eqs. (13), (14) fail for large s when the chain diameter D is nonzero, and excluded volume hence is relevant. Then the asymptotic behavior of $C(s)$ is a power law [63]

$$C(s) \propto s^{-\beta}, \beta = 2(1-\nu) \approx 0.82 \quad (d = 3), \text{ or } \quad \beta = 2(1-\nu_2) = 1/2 \quad (d = 2). \tag{15}$$

While for flexible polymers, where ℓ_p is of the order of the bond length ℓ_b, Eqs. (13), (14) break down at distances s corresponding to a few bond lengths only, for semiflexible polymers with $\ell_p \gg \ell_b$, Eq. (14) holds as long as $s \ll 2\ell_p$. In $d = 3$, however, excluded volume matters only for length scales

s along the chain of the order $s^* = \ell_p n_p^* = \ell_p^3/D^2$, however, and thus Eq. (13) has a more extended range of validity. All these relations, Eqs. (13) - (15), assume distances $s \ll L$.

When both ℓ_p and D are large and of the same order (as is the case for bottlebrush polymers [35, 39], dendronized polymers [41–43], etc.), one observes a slow and extended crossover from Eq. (13) to Eq. (15).

The end-to-end distance square can be expressed in terms of $C(s)$ as [5]

$$\langle [R(L)]^2 \rangle = \int_0^L ds \int_0^L ds' C(|s - s'|) \tag{16}$$

and the gyration radius

$$\langle R_g^2 \rangle = (2L^2)^{-1} \int_0^L ds \int_0^L ds' \langle [R(s - s')]^2 \rangle \quad . \tag{17}$$

Working out these integrals, one can describe explicitly the crossover from rod-like to Gaussian behavior [50, 64]

$$\langle [R(L)]^2 \rangle / (2\ell_p L) = 1 - [1 - \exp(-n_p)]/n_p, \quad d = 3 \tag{18}$$

$$6\langle R_g^2 \rangle / (2\ell_p L) = 1 - 3/n_p + 6/n_p^2 - 6[1 - \exp(-n_p)]/n_p^3, \quad d = 3, \tag{19}$$

while in $d = 2$ the analogous results are [5]

$$\langle [R(L)]^2 \rangle / (4\ell_p L) = 1 - 2[(1 - \exp(-n_p/2)]/n_p, \tag{20}$$

$$3\langle R_g^2 \rangle / (2\ell_p L) = 1 - \frac{6}{n_p}\Big[1 - \frac{4}{n_p}\Big(1 - \frac{1 - \exp(-n_p/2)}{n_p/2}\Big)\Big]. \tag{21}$$

As emphasized above {Eq. (9)}, for large ℓ_p Eqs. (18), (19) do have a well-defined range of applicability, while Eqs. (20), (21) can be used only for the rod-like regime, since a regime of Gaussian behavior in $d = 2$ does not occur [58–60].

Given that close enough to the adsorption threshold the polymer configuration is still essentially three dimensional since the ratio of $\langle R_g^2 \rangle_\perp / \langle R_g^2 \rangle_{||}$ at the threshold is of order unity {Eq. (8)}, it is plausible that the Kratky-Porod model can still be used to locate the position of the adsorption threshold. An extensive analytical theory along such lines was presented by Semenov [52], and later complemented by numerical calculations [53]. These theories assume a square-well adsorption potential of range Δ and depth u, and predict that the adsorption threshold then is [53], for $\Delta \ll \ell_p$

$$u^{\rm cr}/k_B T \approx 0.7797 \ell_b / (\ell_p \Delta^2)^{1/3}. \tag{22}$$

Semenov [52] also predicted that the fraction of adsorbed monomers within the range of the adsorption potential scales as

$$f \approx (\ell_p/\Delta)^{4/3} \tau, \quad 0 < \tau < \tau^* = (\Delta/\ell_p)^{4/3}, \tag{23}$$

while for $\tau > \tau^*$ a saturation at $f = 1$ sets in. However, also in the region $\tau^* \ll \tau \ll \tau^{**}$ long loops away from the surface still occur, although most of the monomers are attached to the surface, and $\tau^{**} = (\Delta/\ell_p)^{2/3}$. The crossover at τ^{**} then shows up in the decay of the monomer concentration profile $c(z)$ far from the surface, which is always exponential, $c(z) \propto \exp(-z/h)$, with

$$h \approx \begin{cases} \Delta/\tau \quad , & 0 < \tau < \tau^* \\ \Delta(\ell_p/\Delta)^{2/3}/\tau^{1/2} \quad , & \tau^* < \tau < \tau^{**} \\ \Delta/\tau^{3/2} \quad , & \tau^{**} < \tau. \end{cases} \tag{24}$$

In the regime $0 < \tau < \tau^{**}$ the chains are "weakly adsorbed" which means $h < \ell_p$ while $\tau > \tau^{**}$ implies strong adsorption. Semenov [52] predicts a triple layer structure of the adsorbed chains, for $0 < z < \Delta$ adsorbed monomers being in "trains", and in the "proximal layer" flat wormlike loops nearly parallel to the surface should occur, while in the distal layer ($\ell_p < z < h$) coil-like semiflexible loops occur. As a caveat we mention, however, that all these predictions apply in the limit of infinitely long chains and neglecting excluded volume effects only. For finite contour length, Eqs. (23), (24) should hold approximately for $L > \ell_p(\ell_p/\Delta)^{2/3}$. Clearly, for large ℓ_p this requires to consider extremely long chains. For smaller L Semenov [52] predicts a rounding of the transition over a range that scales inversely with $Lu^{\rm cr}/k_BT$. Finally, we mention the power law behavior of $c(z)$ at the adsorption transition [52]

$$c(z) \propto (z/\ell_p)^{-4/3}\,, \; \Delta < z < \ell_p. \tag{25}$$

Of course, due to the neglect of excluded volume the theory cannot (and does not) make any prediction for the lateral linear dimensions $\langle R_g^2 \rangle_{||}^{1/2}$ of the adsorbed chains.

III. MODEL AND COMMENTS ON THE SIMULATION METHODS

We consider a bead-spring model for a polymer chain where the effective monomeric units interact with a purely repulsive Weeks-Chandler Andersen (WCA)-type interaction [65]

$$U^{\rm WCA}(r) = 4\epsilon[(\sigma/r)^{12} - (\sigma/r)^6 + 1/4], \quad r < r_c = 2^{1/6}\sigma, \tag{26}$$

choosing the strength $\epsilon = k_BT = 1$, and the range $\sigma = 1$ serves as length unit; $U^{\rm WCA}(r > r_c) \equiv 0$. This interaction acts between any pair of monomers, a distance r apart, and ensures the presence of excluded volume (EV). The bonding of subsequent monomers along the chain is ensured by the finitely extensible nonlinear elastic (FENE) potential [66],

$$U^{\rm FENE}(r) = -0.5kr_0^2 \ln[1 - (r/r_0)^2], \quad r < r_0, \tag{27}$$

and $U(r > r_0) = \infty$. The constants are chosen $r_0 = 1.5\sigma$, $k = 30\epsilon/\sigma^2$, as usual. Finally the bond bending potential is chosen as

$$U_b(\theta_{ijk}) = \kappa[1 - \cos(\theta_{ijk})] \tag{28}$$

where θ_{ijk} is the bond angle formed between the two subsequent unit vectors along the bonds connecting monomers i with j, and j with k, respectively. For large stiffness $\kappa \gg k_BT$ this potential is essentially harmonic in θ_{ijk}, $U_b(\theta_{ijk}) \approx \frac{1}{2}\kappa\theta_{ijk}^2$, and hence the model Eqs. (26), (28) can be viewed as a discretized version of the Kratky-Porod model, Eq. (11), but extended by allowing for excluded volume between any pairs of effective monomers through $U^{\rm WCA}(r)$. The effective bond length ℓ_b between nearest neighbors along the chain, resulting from the combined effect of $U^{\rm FENE}(r)$ and

$U^{\mathrm{WCA}}(r)$ for bonded monomers, turns out to be very close to unity (a slight dependence of ℓ_b on chain length, stiffness, and strength of the adsorption potential is of relative order 10^{-3} or smaller). Eqs. (26), (28) have been used to study liquid crystalline ordering in solutions of semiflexible polymers [67–70]. Studying with this model the orientational correlation function $C(s)$, one finds that Eq. (13) indeed holds for distances s of order of ℓ_p, or smaller, provided $\ell_p \gg 1$. Note that in Eqs. (11), (21) s is a continuous variable, while in our model only discrete distances $s_n = n\ell_b$, $n = 1, 2, \cdots$, are possible. In practice, it is convenient to estimate ℓ_p from the initial slope of $C(s)$, which in the discrete case implies to define an effective decay length ℓ_p^{eff} as

$$\ell_p^{\mathrm{eff}}/\ell_b = -1/\ln\langle\cos\theta_{ijk}\rangle, \tag{29}$$

where the average $\langle\cdots\rangle$ includes both a thermal average and an average over all the bond angles along the simulated chain. Finally we note that the contour length simply is $L = (N-1)\ell_b$; the integer number N of monomers in the chain here is referred to as "chain length".

When one uses Eq. (29) also in $d = 2$, one finds [58–60] $2\kappa/k_BT$, i.e. twice the value applicable in $d = 3$ {Eq. (13)}, as stated in Eq. (14). This doubling of the decay length is straightforwardly understood in the framework of our model, noting that $\langle\cos\theta_{ijk}\rangle \approx 1 - \langle\theta_{ijk}^2\rangle/2$ for large κ and hence $\ell_p^{\mathrm{eff}}/\ell_b \approx 2/\langle\theta_{ijk}^2\rangle$. Treating all bond angles as equivalent, we estimate $\langle\theta^2\rangle$ simply by choosing the z-axis along the direction of the direction of the first bond and use polar coordinate (θ, ϕ) to write

$$\langle\theta^2\rangle = \int_0^{2\pi} d\phi \int_0^{\pi} d\theta \sin\theta e^{-U_b(\theta)/k_BT}\theta^2 / \int_0^{2\pi} d\phi \int_0^{\pi} d\theta \sin\theta e^{-U_b(\theta)/k_BT} \tag{30}$$

in $d = 3$, while an equivalent expression in $d = 2$ is

$$\langle\theta^2\rangle = \int_0^{\pi} d\theta d e^{-U_b(\theta)/k_BT}\theta^2 / \int_0^{\pi} d\theta e^{-U_b(\theta)/k_BT} \tag{31}$$

Recalling $U_b(\theta) \approx \frac{1}{2}\kappa\theta^2$, the resulting integrals are elementary and readily lead to the decay lengths ℓ_p {Eq. (13)} and $2\ell_p$ {Eq. (14)} when Eq. (29) is used.

Eqs. (26) - (28) do not constitute the only possible choice of a coarse-grained model for semiflexible polymers. Kierfeld et al. [71–73] used the semiflexible harmonic chain model, discretizing the Kratky-Porod model into a sequence of $N-1$ bond vectors $\vec{t}_i$, whose length is controlled by a (rather strong) harmonic potential, and the bonding potential is also equivalent to Eq. (28). In the limit where $N \to \infty$ but L/ℓ_p stays fixed this model must reduce strictly to the Kratky-Porod model. However, it does neither allow a useful study of the crossover to flexible polymer behavior as far as excluded volume is not included, nor is it appropriate for stiff chains in $d = 2$, see Eq. (10). So this model would not have been useful for our purposes.

A physically very reasonable model similar to Eqs. (26)- (28) was used by van der Schoot et al. [74, 75]. Using a different choice for the binding potential of subsequent monomers (instead of Eq. (27)) they obtain ℓ_b significantly smaller than the bead diameter σ, so the beads strongly overlap and the local structure of the chain is a flexible rod rather than a chain of tangent spheres. This model is presumably a very good coarse-grained model for semiflexible biopolymers such as ds DNA, F-actin, etc.; but it is inconvenient for the study of chains with $L \gg \ell_p$, or the study of the crossover to flexible chains. Of course, the choice of a coarse-grained model always necessitates compromises, and we feel that for the purpose of the present study the model defined by Eqs. (26)- (28) is a reasonable choice.

The adsorbing surface is modelled by a planar structureless impenetrable wall located in the xy plane at $z = 0$ at which a potential $U_{\rm wall}(z)$ depending only on the distance from the surface acts,

$$U_{\rm wall}(z) = \epsilon_{\rm wall}\Big(\frac{5}{3}\Big)\Big(\frac{5}{2}\Big)^{2/3}\Big[\Big(\frac{\sigma_w}{z}\Big)^{10} - \Big(\frac{\sigma_w}{z}\Big)^{4}\Big] \quad . \tag{32}$$

This potential has a minimum of depth $U_{\rm wall}(z_{\rm min}) = -\epsilon_{\rm wall}$ at $z_{\rm min}/\sigma_w = (5/2)^{1/6}$. The range Δ of this potential can be defined as the interval Δz of the regime where $U_{\rm wall}(z) < -\epsilon_{\rm wall}/2$, i.e. $\Delta/\sigma_w = 0.55$. For simplicity, we have taken $\sigma_w \equiv \sigma(= 1)$. We feel that the choice Eq. (32) is a bit more realistic than the square well potential used in most previous work (e.g. [52, 53, 72, 73]). In particular, a choice, using Δ as large as of order ℓ_p can be realized only in exceptional cases, such as absorption of polymers from solution into polymer brushes, whose height h may be controlled by the chain length of the polymers forming the brush [76–78]. The present model {Eq. (32)} has been also found useful for study of solutions of semiflexible polymers confined by attractive walls [79, 80].

Molecular Dynamics (MD) methods [81] are used in the constant temperature ensemble, using a standard Langevin thermostat [66] as in our previous work on bulk solutions of semiflexible polymers [68–70]. Note, however, that for simulations of rather long single semiflexible chains it would not be convenient to us a $L_x \times L_y \times L_z$ box (with periodic boundary conditions in x, y directions and a repulsive wall at $z = L_z$), as done for simulations of confined solutions [79, 80]: one would need prohibitively large boxes (with linear dimensions L_x, L_y, L_z), to avoid that the chain interacts with its periodic images, causing significant systematic errors. Thus for $N = 250$, 500, and 750 we have used a simulation in "infinite space", where for the calculation of forces a Verlet linked cell list [81] is used to identify the monomers a given monomer interacts with. The grafted chain end is put at the point ($x = 0$, $y = 0, z = 1$). Actually one can run $\mathcal{N}$ chains in parallel in the same volume, which simply are not interacting at all with each other, but this allows for a straightforward parallelization when one uses the HOOMD-blue software [82, 83] on graphics processing unit (GPUs). Typically $\mathcal{N} = 50$ is used, and the MD time step was chosen $\delta = 0.002\tau_{\rm MD}$ where $\tau_{\rm MD} = \sqrt{m\sigma^2/\epsilon} = 1$ (choosing the monomer mass $m = 1$) is the relevant time unit.

The length of the MD runs typically was extended up to 10 million MD time units. Note that the slow relaxation of the chain conformations is a very serious limitation of our simulations, preventing us to simulate chains longer than $N = 750$. As is well known, for flexible polymers the relaxation time $\tau_{\rm rel}$ scales as [44]

$$\tau_{\rm rel} = W^{-1}N^{2\nu+1}, (d = 3), \tau_{\rm rel} \approx W^{-1}N^{2\nu_2+1}(d = 2) \tag{33}$$

where W^{-1} is the typical time it takes for a monomer to move over a distance of its own diameter (for simplicity, prefactors of order unity are not considered here). When excluded volume forces are shut off (NoEV), i.e. in the Gaussian chain limit, $\nu = \nu_2 = 1/2$ needs to be used in Eq. (33). However, when chain stiffness is pronounced, the relaxation times get significantly enhanced. Huang et al. [59] found in $d = 2$

$$\tau_{\rm rel} \approx W^{-1}\kappa^{1/2}N^{5/2} \quad , \tag{34}$$

and putting $W^{-1} = \tau_{\rm MD}$, $\kappa = 25$, one would find $\tau_{\rm rel} \approx 28$ million times $\tau_{\rm MD}$ for $N = 500$. In $d = 3$, we profit from the fact that there occurs the intermediate Gaussian regime, for $L \ll L^* \approx \ell_p^3/\ell_b^2 = \kappa^3\ell_b$. So for $\kappa = 25$, L^*/ℓ_b is of order 15000, and hence $N = 500$ clearly is in the regime where excluded volume effects should be negligible, and then [84]

$$\tau_{\rm rel} \approx W^{-1}\kappa N^2 \tag{35}$$

which yields about 6 millions times $\tau_{\rm MD}$. These estimates imply that indeed 10 millions times $\tau_{\rm MD}$ is about enough to have a single well equilibrated chain conformation. Since quantities such as $\langle R^2\rangle$

exhibit the problem well-known as [85] lack of selfaveraging, the relative accuracy of $\mathcal{N}$ runs of length $\tau_{\rm rel}$ to estimate $\langle R^2\rangle$ is only about $\sqrt{2/\mathcal{N}}$ ($\approx 20\%$ if $\mathcal{N}=50$). Due to this problem, we do not base our analysis on numerical data for $\langle R^2\rangle$; for $\langle R_g^2\rangle$ the problem fortunately is a bit less serious, but still relative errors of up to 10% in unfavorable cases still did occur. Only for quantities based on local observables, such as the adsorbed fraction of monomers f, self-averaging helps and much better statistical accuracy is reached. Yet also for such quantities well equilibrated chain configurations (requiring runs of length of the order of $\tau_{\rm rel}$) are mandatory.

We add a caveat: in the regime of $\epsilon_{\rm wall}$ where a long chain is only weakly adsorbed {e.g. Fig. 1}, the conformation contains trains and loops of various sizes. Short loops are predicted [52] to have monomer coordinates $z_i \ll \ell_p$, while long loops extend far away from the surface. For equilibrating such structures, the monomers of the trains intermediate between the loops must unbind from the surface. It is likely that such processes lead to an enhancement of the relaxation times near the adsorption transition, i.e. a "critical slowing down" occurs, as is familiar from other phase transitions [86]. However, a study of the (reversible) dynamics of the adsorption transition must remain a challenge for future work; at this point we draw attention to very interesting work studying irreversible adsorption of semiflexible polymers [87]. Conformations of irreversibly adsorbed chains are out of equilibrium, and although this problem may affect some of the experiments, it remains out of focus here.

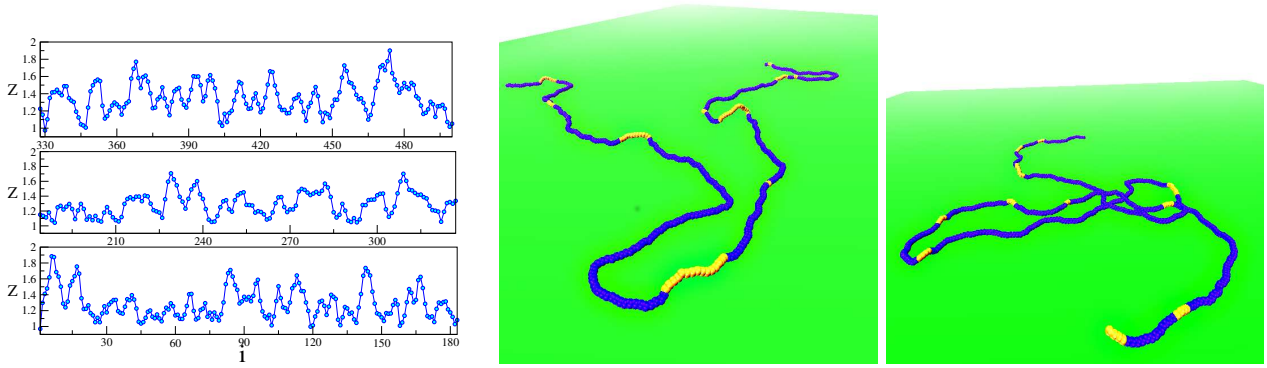

FIG. 2: (a) Conformation of a strongly adsorbed rather stiff chain ($N=500, \kappa=64, \epsilon_{\rm wall}=0.80$) showing the z-coordinates z_i of all monomers i vs monomer index i. Each monomer position is shown by a dot, and subsequent monomers are connected by straight lines. (b) Projections of selected conformations of strongly adsorbed moderately stiff chains ($N=500, \kappa=16, \epsilon_{\rm wall}=0.80$) into the xy-plane, with excluded volume (left part), and without excluded volume interaction (NoEV) (right part). Loops are shown in yellow and trains - in dark blue. Typically, the parallel gyration radii components $R^2_{g||}$ are somewhat smaller in the NoEV case, and their projections onto the xy-plane exhibit more chain crossings than in the case where EV is included.

The problem of loops versus trains is less relevant for strongly adsorbed chains since then loops (for large κ) are extremely rare. As an example, Fig. 2a shows the snapshot of the z coordinates of a typical chain configuration for $N=500$, $\kappa=64$ at $\epsilon_{\rm wall}=0.8$. One sees that all z-coordinates z_i of this chain are in the range from about $z=1$ to $z=1.9$, i.e., no loops at all are present. Typically z-coordinates move from some local minimum at small z in the range $1<z<1.3$, a few steps upwards to reach a local maximum in the range of $1.7<z<1.9$, and then recede again. We shall interpret this behavior in terms of the *deflection length* concept [54] in Sec. V.

In the case of Fig. 2a) we plot z as a function of the monomer index i along the chain (for the sake of clarity the interval from $i=1$ to $i=N$ is divided into three parts) in order to show that $z(i)$ reaches local minima and maxima, typically separated from each other by several steps. The mean

distance between such extrema can be taken as an estimate of the deflection length. The average gyration radius components $\langle R_g^2\rangle_{||} \approx 1.2\times 10^4$, $\langle R_{g_z}^2\rangle \approx 0.05$ also imply that all z_i are within a range of about $\Delta z \approx \pm 0.2$ of their average, and typical linear dimensions of this quasi-two-dimensional polymer are of the order of 10^2. In contrast, for less stiff chains (Fig. 2b) the xy-projections do reveal that the conformation of the polymer no longer is rod-like, but rather a loose coil. The snapshots suggest that in the NoEV case there occur more chain intersections in the chain conformation than in the case where EV is present (and each intersection point actually means that in three-dimensional conformation there is a small loop, since strict intersections in the presence of EV are completely avoided).

The comparison between the cases with EV and without EV in Fig. 2b, illustrates one major advantage of the simulation approach, namely the effect of particular interactions can be stringently tested, by switching them on or off, which in an experiment would not be possible. Also individual chain conformations can be analyzed in detail. Of course, one must not rely in one's conclusions on observations of particular conformations only; but the observation that with EV the chain radii are clearly larger since EV tends to swell the polymer coils emerges also from the averages. For instance, in the case of Fig. 2b we find $\langle R_{||}^2\rangle \approx 6030$ with EV and $\langle R_{||}^2\rangle \approx 3780$ without EV.

Unlike some theoretical studies of detachment kinetics of strongly adsorbed chains [88], where it is assumed that all monomers of the adsorbed part are strictly localized in the plane $z = z_{min}$, we find, cf. Fig. 2a, that vertical fluctuations in perpendicular direction do occur.

IV. LOCATING THE ADSORPTION TRANSITION

In the summary of the theory (Sec. II) we have emphasized that a sharp adsorption threshold occurs only in the limit $N \to \infty$. This presents a difficulty for the simulations, which are limited to rather moderate chain lengths only. As a first test for our procedures, we study next the case of completely flexible polymers, choosing $\kappa = 0.1$ for this purpose. Fig. 3a shows a log-log plot of f vs N for various choices of $\epsilon_{\rm wall}$, and Fig. 3b a plot of $\langle R_{g\perp}^2\rangle/\langle R_{g||}^2\rangle$. Note that the precise definition of the adsorbed fraction that we apply uses the monomer density profile $\rho(z)$ as

$$f = \int_0^\infty dz U_{\rm wall}(z)\rho(z) / \int_0^\infty dz U_{\rm wall}(z) \tag{36}$$

with the normalization $\int_0^\infty dz\rho(z) = 1$. As expected, in the non-adsorbed region $f(N)$ decreases for large enough N towards zero distinctly faster than $1/\sqrt{N}$, while in the regime of adsorbed chains the decay slowly bends over in order to ultimately settle down at nonzero asymptotes. For $N < 10^3$ neither the asymptotic $1/N$ decay in the nonadsorbed regime nor the plateau $f_\infty = \lim_{N\to\infty} f(N)$ are clearly reached in the transition regime, but from Fig. 3a a value $\epsilon_{\rm wall}^{\rm cr} \approx 0.65$ seems likely, since for $\epsilon_{\rm wall} = 0.65$ the effective exponent on this log-log plot for large N is close to the theoretical value, $1 - \varphi \approx 0.52$ {cf. Eqs. (5), (6)}. Gratifyingly, the data for f are reasonably well compatible with the predicted scaling behavior, Eq.(5), see Fig.3c. This estimate is corroborated by the crossing of the ratios of the radii for different N (Fig. 3b).

Of course, it is clear that for the available not very large N the accuracy with which $\epsilon_{\rm wall}^{\rm cr}$ can be located is rather modest, but this is expected in view of the experience with the lattice model [15] where much longer chains were available. Also the expected change from $\langle R_g^2\rangle_{||} \propto N^{2\nu}$ to $\langle R_g^2\rangle_{||} \propto N^{2\nu_2}$ (with $\nu \approx 0.59; \nu_2 = 0.75$) in this range of N cannot yet be verified with meaningful

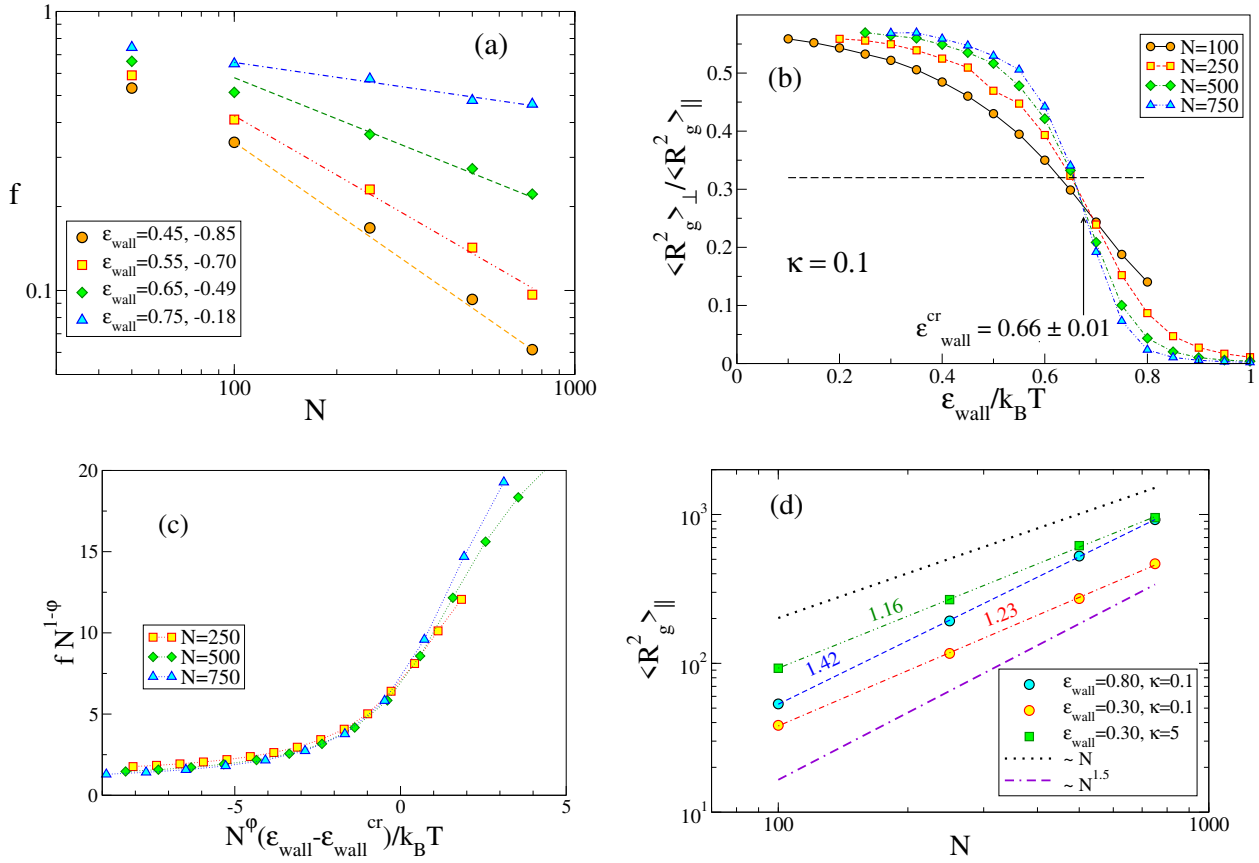

FIG. 3: a) Log-log plot of f vs N for the case $\kappa = 0.1$ and several choices of $\epsilon_{\rm wall}$ as indicated. Straight lines indicate effective exponents (quoted in the legend), if one assumes a power-law decay. b) Plot of $\langle R_g^2\rangle_\perp/\langle R_g^2\rangle_{||}$ vs. $\epsilon_{\rm wall}$ for the case $\kappa = 0.1$ and several choices of N, $N = 100, 250, 500$ and 750. The horizontal broken straight line indicates the theoretical universal value $F(0) = 0.32$ at the transition, where for large enough N all curves should cross. This crossing criterion is compatible with an estimate $\epsilon^{\rm cr}_{\rm wall} = 0.66 \pm 0.01$. c) Scaling plot $fN^{1-\varphi}$ of the adsorbed fraction f versus N^φ $(\epsilon_{\rm wall} - \epsilon^{\rm cr}_{\rm wall})$ for the same four choices of N as used in (a,b), for the choices $\varphi = 0.48$, $\epsilon^{\rm cr}_{\rm wall} = 0.66$. d) Log-log plot of $\langle R_g^2\rangle_{||}$ in the adsorbed phase $\epsilon_{\rm wall} = 0.8$ and in the nonadsorbed phase ($\epsilon_{\rm wall} = 0.3$), also the case $\epsilon_{\rm wall} = 0.3$, $\kappa = 5$ is included. Slopes indicate effective exponents

precision (see Fig. 3d), but it is clear that the adsorbed chains have much larger linear dimensions parallel to the wall than the non-adsorbed ones.

For moderate stiffness ($\kappa = 5$, $\kappa = 8$) the behavior is still in many respects similar to the case of flexible polymers (Fig. 4). It is interesting that in this range of κ the location of the adsorption is hardly distinct from the case of flexible chains: $\epsilon^{\rm cr}_{wall}(\kappa = 5) \approx 0.66 \pm 0.02$ and $\epsilon^{\rm cr}_{wall}(\kappa = 8) \approx 0.63 \pm 0.01$. This range of stiffness hence clearly is outside the range where the theories of Semenov et al. [52, 53] apply. It is also interesting to note that there the data for $\langle R_g^2\rangle_\perp/\langle R_g^2\rangle_{||}$ are clearly not compatible with a common intersection point at a ratio of 0.32, at least not for the accessible range of chain lengths. Tentatively one might conclude that a unique intersection point rather could be found for a ratio in the range from 0.20 to 0.25. One might expect that this behavior reflects the suggestion that at the adsorption transition, where the chains are still three-dimensional in their character, excluded volume is not yet felt much, for the available chain lengths. Although, the actual data for $\langle R_g^2\rangle_{||}$ in the non-adsorbed phase do not corroborate this suggestion (Fig. 3d), one must be careful since Eq. (19) implies a very slow crossover from rodlike behavior to Gaussian behavior, and one decade in N hence may not suffice to clarify any asymptotic exponent.

For $\kappa = 16$ and $\kappa = 25$ the plots log f vs. log N and $\langle R_g^2\rangle_\perp/\langle R_g^2\rangle_{||}$ vs. ϵ_{wall} look similar to those shown for $\kappa = 5$ and $\kappa = 8$, with the important exception that now a significant reduction of $\epsilon^{\rm cr}_{\rm wall}$

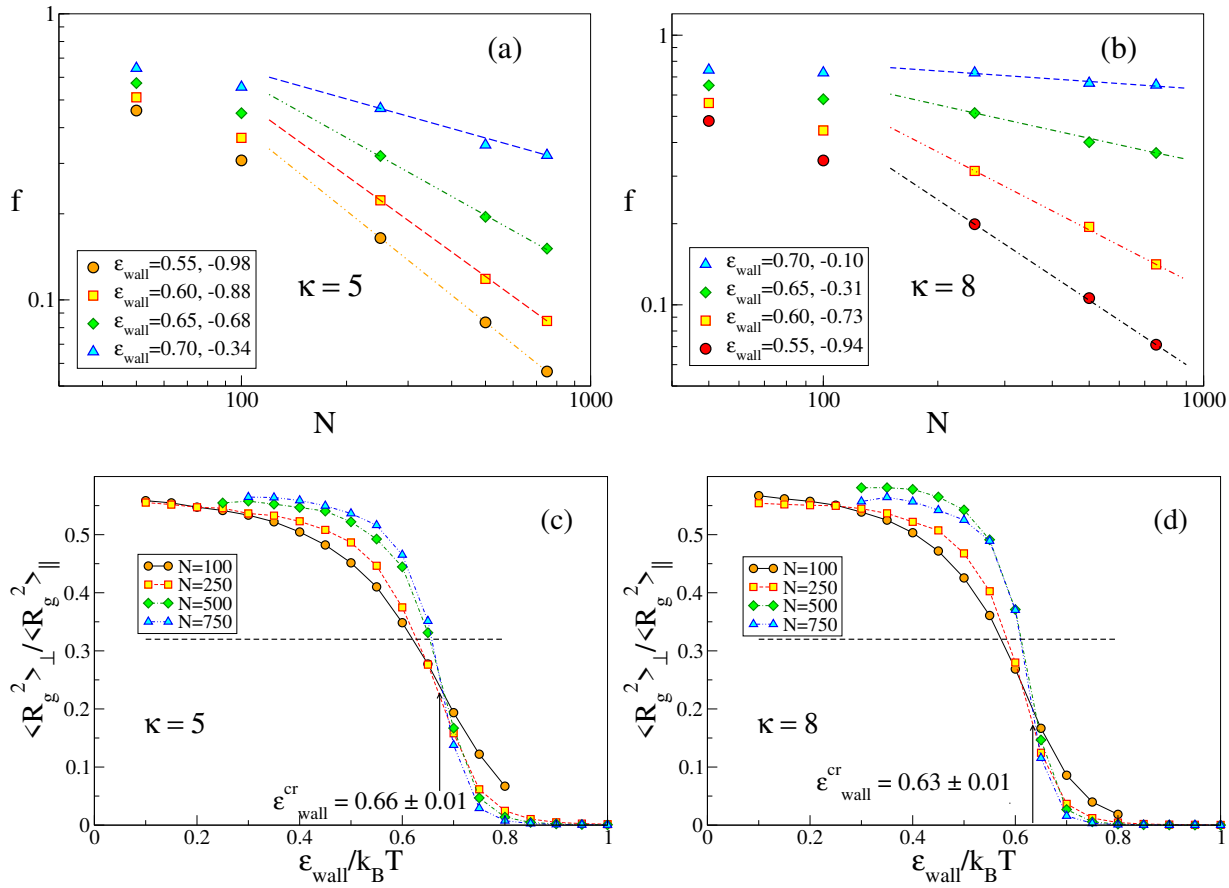

FIG. 4: Log-log plots of f vs N for $\kappa = 5$(a) and $\kappa = 8$ (b). Broken straight lines indicate power laws with effective exponents, which are quoted in the legend. Plot of $\langle R_g^2\rangle_\perp/\langle R_g^2\rangle_{||}$ vs. $\epsilon_{\rm wall}$ for $\kappa = 5$ (c) and $\kappa = 8$ (d). Horizontal straight line indicates the theoretical universal value of the crossing point $F(0) = 0.32$ {cf. Eq.(8)}, for the case where excluded volume is fully effective.

occurs. We find $\epsilon^{\rm cr}_{\rm wall}(\kappa = 16) \approx 0.53 \pm 0.01$ and $\epsilon^{\rm cr}_{\rm wall}(\kappa = 25) \approx 0.48 \pm 0.01$. Some data for f vs. $\epsilon_{\rm wall}$ for these cases were already given in our preliminary publication [62], and to save space we do not repeat this material. We only mention that with increasing κ there is a strong tendency that the curves f vs. ϵ_{wall} for different N intersect in a narrow region and their maximum slope $(\partial f/\partial\epsilon_{wall})_{\rm max}$ occurs in this region and strongly increases with N. Fig. 5 gives some examples for $\kappa = 32$ and $\kappa = 64$ (Data for $\kappa = 50$ have also been taken, and look similar to those shown, and hence are not displayed here to save space). We have included here the orientational order parameter η defined as

$$\eta = \frac{3}{2}\langle \cos^2\zeta\rangle - \frac{1}{2} \tag{37}$$

where ζ is the angle between a bond vector and the z-axis. The average $\langle\cdots\rangle$ includes an average over all the bond vectors of the chain. While η is less useful for flexible chains, since in the adsorbed phase near the transition many bonds are oriented perpendicular to the surface (and for such a bond $\cos^2\zeta = 1$), for adsorbed semiflexible chains in the adsorbed phase most bonds are approximately parallel to the surface (and hence $\cos^2\zeta = 0$) and this order parameter is certainly useful [62]. E.g., for the case shown in Fig. 2a $\eta = -0.4855$, close to the perfect saturation value $-1/2$ (while $f \approx 0.99986$

then). On the other hand, for the case shown in Fig. 1 ($\kappa = 16$, $\epsilon_{\rm wall} = 0.65$, $N = 500$) $\eta = -0.3943$ and $f = 0.9332$. In the latter case, switching off EV would enhance the order ($\eta = -0.3943$ and $f = 0.9514$); this observation is already an indication that in the transition region from non-adsorbed mushrooms to weakly adsorbed "pancakes" the description based on the Kratky-Porod model without EV is not quantitatively reliable.

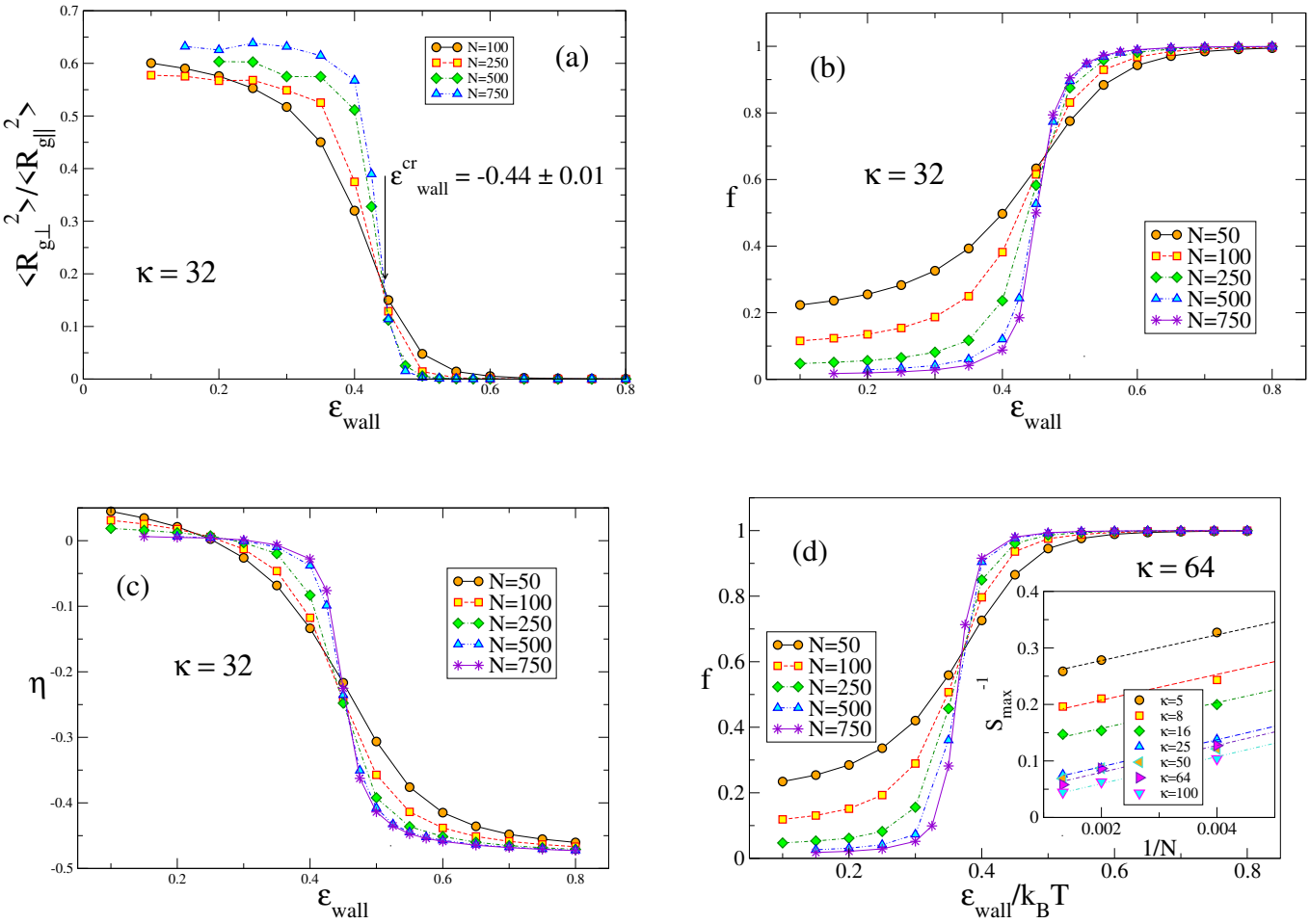

FIG. 5: Plots of $\langle R_g^2\rangle_\perp\rangle/\langle R_g^2\rangle_{||}$ (a), $f(b)$ and orientational order parameter $\eta(c)$ vs $\epsilon_{\rm wall}$ for the case $\kappa = 32$. Part (d) shows a plot of f vs. $\epsilon_{\rm wall}$ for the case $\kappa = 64$. Inset of Part (d) shows estimates for the inverse, S_{max}^{-1}, of the maximum slope $S_{max} = [\partial f/\partial\epsilon_{\rm wall}]^{-1}_{\rm max}$ versus $1/N$, for several choices of κ are indicated.

The case of $\kappa = 64$ (Fig. 5d) is reminiscent of the behavior of a first-order transition rounded by finite size, a situation familiar from the Monte Carlo studies of phase transitions [85]. Adapting the corresponding considerations to the present case, the assumption of a 1st order transition would imply that the free energy of the adsorbed chain is (c is a constant of order unity)

$$\Delta F_{\rm ads} = -c\epsilon_{\rm wall}L - TLs_{\rm ads}, \tag{38}$$

while (neglecting the adsorption enthalpy for the mushroom state) the free energy of the non-adsorbed chain (n.a) is

$$\Delta F_{\rm n.a.} = -TLs_{\rm n.a.} \tag{39}$$

Note that for simplicity we disregard here possible slight differences of the energy due to the bond potential {Eqs. (26), (27)} between both phases, which would not change the essence of the

argument. Here $s_{\rm ads}$ is the entropy due to the deflection fluctuations per unit length of the chain (i.e., the disorder illustrated in Fig. 2a), while $s_{\rm n.a.}$ is the entropy per unit length in the mushroom state. If Eqs. (38), (39)} can be used up to the transition point at $\epsilon^{\rm cr}_{\rm wall}$, treating near this point $s_{\rm ads}$, $s_{\rm n.a}$ and the prefactor c in the enthalpic term as constants, one finds $\epsilon^{\rm cr}_{\rm wall}/T = (s_{\rm n.a} - s_{\rm ads})/c$. For finite L, both phases contribute with weights proportional to the corresponding Boltzmann factors, i.e. $w_{\rm n.a.} \propto \exp(-\Delta F_{\rm n.a.}/T)$, $w_{\rm ads} \propto \exp(-\Delta F_{\rm ads}/T)$, and hence the adsorbed fraction becomes

$$f = [1 + \exp(-L\delta)]^{-1}, \quad \delta = c(\epsilon_{\rm wall} - \epsilon^{\rm cr}_{\rm wall})/T \tag{40}$$

From Eq. (40) one would predict that curves f vs. $\epsilon_{\rm wall}$ for different N all should intersect at the point $\epsilon_{\rm wall} = \epsilon^{\rm cr}_{\rm wall}$, $f = 1/2$, and the maximum slope (which occurs at this transition point) is proportional to L. The actual data crossing at about $f \approx 0.6$ for $N = 64$, indicates, however, that the true behavior is less simple. Also the inverse maximum slope S^{-1}_{max} (cf. inset in Fig.5d) stays nonzero for $N \to \infty$ but systematically decreases with κ. Indeed, theoretical arguments [52] suggest that the adsorption transition becomes of first-order strictly only in the limit $\kappa \to \infty$ (and then $\epsilon^{\rm cr}_{\rm wall} \to 0$, however). So it is likely that in a very narrow region of $\epsilon_{\rm wall}$ around $\epsilon^{\rm cr}_{\rm wall}$ the sharp entropy

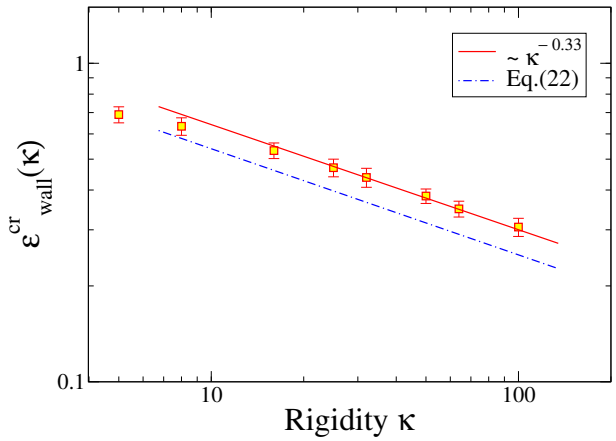

FIG. 6: Log-log plot of $\epsilon^{\rm cr}_{\rm wall}$ (dots with error bars) versus κ. Straight line indicates the theoretical slope, $-1/3$. The broken line represents the theoretical prediction [53] Eq. (22), when $\Delta = 0.55$ is used as a corresponding value for the range of our potential {Eq. (32)}.

jump from $s_{\rm n.a.}$ to the smaller value $s_{\rm ads}$ is replaced by a rapid but continuous change. Much longer chains than available to us would be needed to resolve this.

The estimates $\epsilon^{\rm cr}_{\rm wall}$ from our analysis still contain relative errors of several percent

$$\epsilon^{\rm cr}_{\rm wall} = 0.44 \pm 0.01, \quad 0.38 \pm 0.01, \quad 0.36 \pm 0.01, \quad 0.32 \pm 0.015 \tag{41}$$

for $\kappa = 32, 50, 64$ and 100, respectively. Gratifyingly, these findings are compatible with the theoretical prediction [52], $\epsilon^{\rm cr}_{\rm wall} \propto \kappa^{-1/3}$, (see Fig. 6). The prefactor predicted for this relation {Eq. (22)} does not fit our data quantitatively, but this is expected due to the difference between the square well potential used in the theory [52, 53] and our smooth adsorption potential, Eq. (32). The estimates for $\epsilon^{\rm cr}_{\rm wall}$ in our preliminary work, based on a less reliable extrapolation procedure, agree better with Eq. (22), but we consider the present estimates to be more reliable.

V. PROPERTIES OF ADSORBED SEMIFLEXIBLE CHAINS

We have seen in the previous section that near the adsorption transition the finite size of the chain length N causes a nontrivial rounding of the singular critical behavior. Outside of the transition

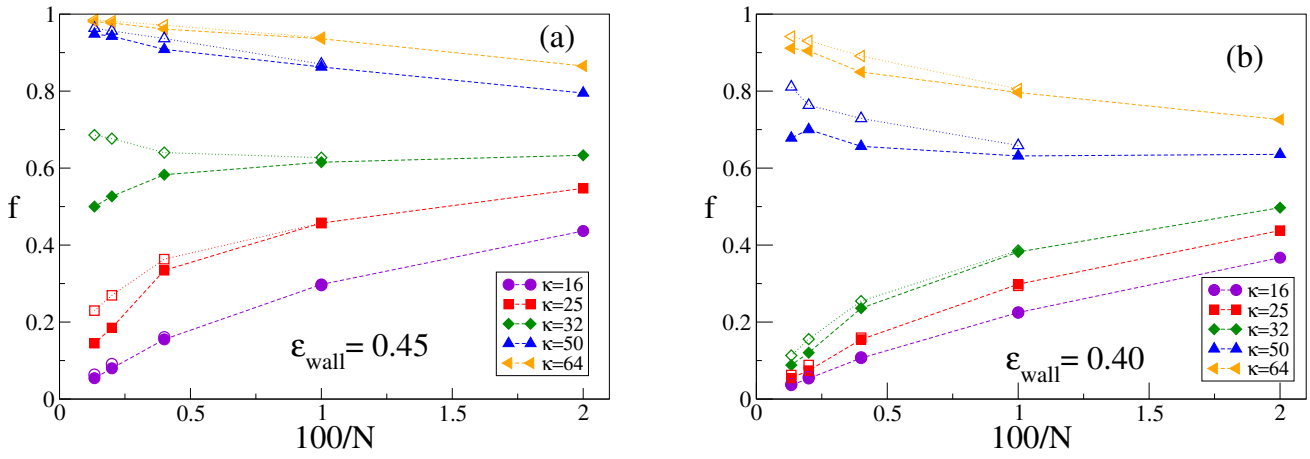

FIG. 7: Plot of f vs $1/N$, for $\epsilon_{\rm wall} = 0.45$(a) and 0.40(b) , for several values of κ, as indicated. Both data with (full symbols) and without excluded volume interactions (open symbols) are included. Note that differences between the EV and NoEV data are pronounced only close to $\epsilon^{\rm cr}_{\rm wall}$, since in the NoEV case $\epsilon^{\rm cr}_{\rm wall}$ is slightly smaller than in the EV case.

region, however, we expect that a simple extrapolation of all chain properties to the limit $N \to \infty$ should be possible. This idea is tested in Figs. 7 and 8.

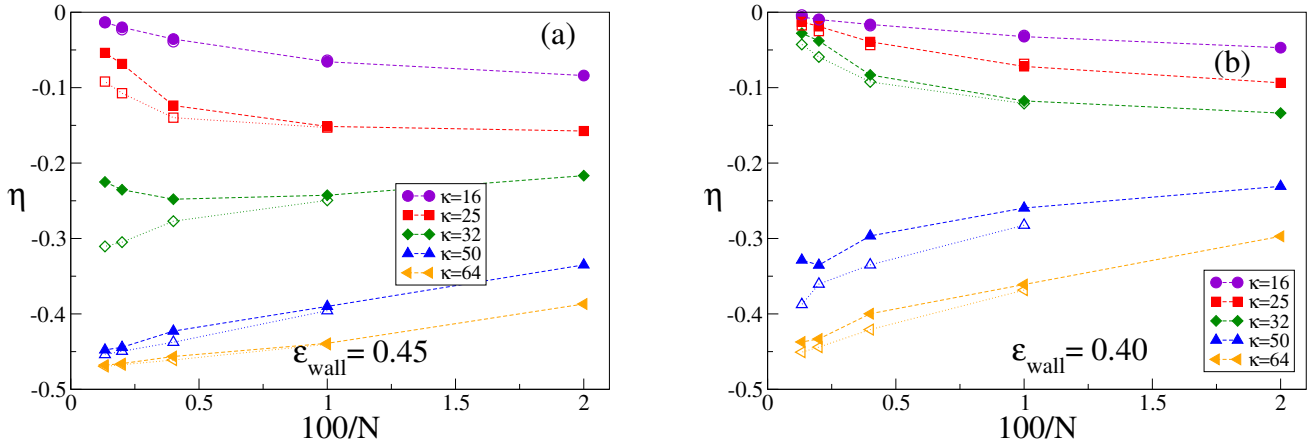

FIG. 8: Plot of η vs. $1/N$, for $\epsilon_{\rm wall} = 0.45$(a) and 0.40(b), for several volumes of κ, as indicated. Both data with (full symbols) and without excluded volume interactions (open symbols) are included. Note that differences between the EV and NoEV data are only pronounced close to $\epsilon^{\rm cr}_{\rm wall}$, since in the NoEV case $\epsilon^{\rm cr}_{\rm wall}$ is slightly smaller than in the EV case.

Fig. 7 shows extrapolation for f, Fig. 8 extrapolations of η, choosing $\epsilon_{\rm wall} = 0.45$ and 0.40 as examples. One can see that in the nonadsorbed region both η and f converge towards zero, as expected, ultimately linear in $1/N$. It is observed that close to the adsorption threshold systematic discrepancies between the data with EV and without EV occur. We find that without EV the adsorption threshold is slightly smaller (but the accuracy of Eq.(41) does not suffice to reliably quantify this effect). Conversely, deep in the phase of adsorbed chains, both order parameters converge to nonzero values, again ultimately linear in $1/N$. The resulting asymptotic order parameters $f_{\rm extr} = \lim_{N\to\infty} f(N)$ and $\eta_{\rm extr} = \lim_{N\to\infty} \eta(N)$ are shown in Fig. 9.

We now return to the observation, Fig.2a, that the localization of the chains in the plane $z = z_{\rm min}$ is not perfect. This means that the picture of the adsorbed chains as a strictly two-dimensional polymer is not fully applicable, and this casts doubt whether or not Eqs. (14), (20), (21) are accurate. Indeed,

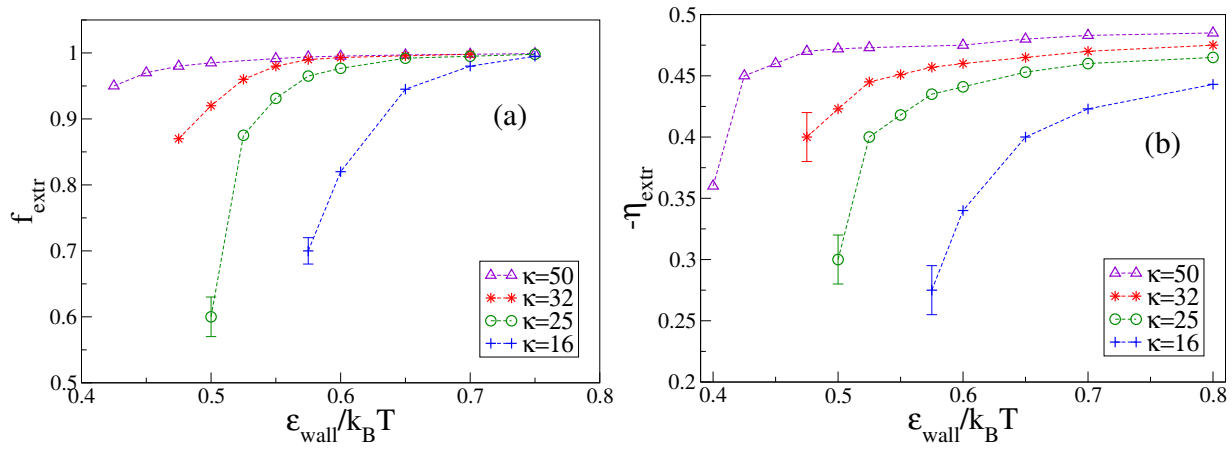

FIG. 9: Extrapolated values of the adsorbed fraction ($f_{\rm extr}$), case (a), and orientational order parameter ($-\eta_{\rm extr}$), case (b), plotted vs. $\epsilon_{\rm wall}$. Note that no meaningful estimates can be found near $\epsilon^{\rm cr}_{\rm wall}(\kappa)$. Lines connecting the points are guides for the eye only. Error bars are only shown when they exceed the size of the symbol.

when we apply Eq. (29) to estimate the effective decay length $\ell_p^{\rm eff}$ of orientational correlations, we find that $\ell_p^{\rm eff}$ is only slightly enhanced over κ, even for strongly adsorbed chains, Fig. (10a).

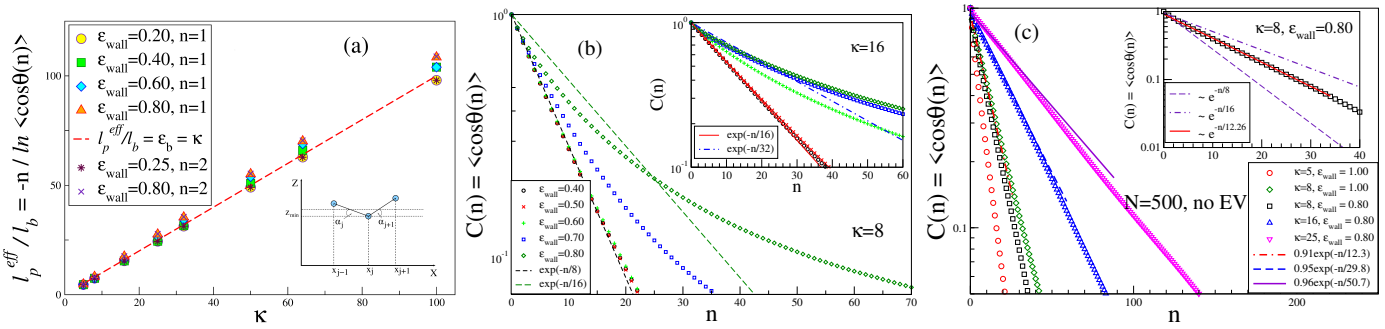

FIG. 10: (a) Plot of the decay length $\ell^{\rm eff}/\ell_p = -n/\ln\langle\cos\theta(n)\rangle$ of an adsorbed chain for $N = 250$ vs. κ, for several choices of $\epsilon_{\rm wall}$, including both choices $n = 1$ (i.e., the angle between neighboring bond vectors is used) and $n = 2$ (i.e., the angle formed between next nearest neighbors bond vector is used). The inset illustrates the geometry of the xy coordinates of two subsequent bonds where the x-axis is chosen such that the bond from $\vec{r}_{j-1}$ to $\vec{r}_j$ lies in the (x, y)-plane. The angles $\alpha_j = \pi/2 - \zeta_j$ are the complements to the polar angles ζ_j of the bond with the z-axis. (b) Autocorrelation function $C(n) = \langle\cos\theta(n)\rangle$ plotted versus the index n characterizing the distance between monomers i, j along the chain ($n = j - i$), for $N = 500$, $\kappa = 8$ (main panel) and $\kappa = 16$ (inset). In the main panel the (theoretical) initial decay laws $\exp(-n/\kappa)$ and $\exp(-n/2\kappa)$ are included (straight lines in the semilog plot). (c) Semilog plot of $C(n)$ vs. n for $N = 500$ and several choices of κ, as indicated, when the excluded volume interaction is shut off. Straight lines show fits to decay laws $C(n) = A\exp(-n/\ell_p^{\rm eff})$ and the fit parameters for the amplitude A and the decay constant $\ell_p^{\rm eff}$ are quoted in the legend. The inset shows a magnification of the initial part of the decay for $\kappa = 8$, $\epsilon_{\rm wall} = 0.8$, comparing the actual data to the three decay laws.

While for a chain in strictly two dimensions the use of Eq. (29) yields $\ell_p^{\rm eff}/\ell_b = 2\kappa/k_BT$ readily [59, 60], this is not the case here. We can understand this fact by considering the geometry of two subsequent bond vectors in more detail (insert of Fig. 10a). Choosing polar coordinates to describe the bond vectors,

$$\vec{r}_j - \vec{r}_{j-1} = \ell_b(-\cos\alpha_j, 0, \sin\alpha_j). \tag{42}$$

$$\vec{r}_{j+1} - \vec{r}_j = \ell_b(\cos\alpha_{j+1}\cos\phi, \cos\alpha_{j+1}\sin\phi, \sin\alpha_{j+1}) \tag{43}$$

and noting that for strongly adsorbed stiff chains the angles α_j, α_{j+1} and ϕ are small, we find that the angle θ between the bonds becomes

$$\theta^2 = \phi^2 + (\alpha_j - \alpha_{j+1})^2. \tag{44}$$

Only when all coordinates z_{j-1}, z_j, z_{j+1} are the same, $\alpha_j - \alpha_{j+1} \equiv 0$, and θ corresponds to a single degree freedom (ϕ) transverse to the chain backbone. But when one moves several steps along the chain, a crossover of the decay of C(s) from an initial decay length ℓ_p to the two dimensional value $2\ell_p$ sets in, and this strictly $d = 2$ value $\ell_p^{\rm eff} = 2\ell_p$ is only found for strongly adsorbed chains, but not for weakly adsorbed ones (Fig. 10b,c). It is seen that for non-adsorbed chains (i.e., the cases $\epsilon_{\rm wall} = 0.4, 0.5, 0.6$ for $\kappa = 8$) $C(n) \approx \exp(-n/\kappa)$ describes the first decade of the decay of $C(n)$ accurately, as expected in $d = 3$ where excluded volume effects play a role only for very large distances (the crossover to the power law Eq. (15) is expected to occur when n becomes of order κ^3). For $\epsilon_{\rm wall} = 0.7$, however, we have a weakly adsorbed chain with initial decay $C(n) \approx \exp(-n/\kappa)$ for $n \leq 5$, and then a region of pronounced curvature on the log-log plot starts. This curvature in our opinion, does not reflect the power law Eqs. (15) that applies to chains that "live" precisely either in $d = 2$ or in $d = 3$. It reflects rather the fact that a weakly adsorbed chain with loops and trains "lives" in between the dimensionalities. For $\epsilon_{\rm wall} = 0.8$, however, the chain is strongly adsorbed, and in $d = 2$ the crossover to the power law Eq. (15) sets in when n exceeds $\ell_p^{\rm eff} \approx 2\kappa = 16$ distinctly. Note that the theoretical decay law $C(n) = \exp(-n/2\kappa)$ deviates slightly but systematically from the actual data also for $n < 2\kappa$, since the actual decay starts out as $C(n) \approx \exp(-n/\kappa)$ for $n = 1, 2, 3$ and then crosses over to $A\exp(-n/\ell_p^{\rm eff})$ near $n = 3, 4$ (see Fig. 10c, insert). The insert in Fig. 10b shows the analogous behavior for $\kappa = 16$; there it is the case $\epsilon_{\rm wall} = 0.6$ which is "in between" the dimensionalities (since $\epsilon_{\rm wall}^{\rm cr} \approx 0.53$ for $\kappa = 16$, $\epsilon_{\rm wall} = 0.7$ then already is a strongly adsorbed case).

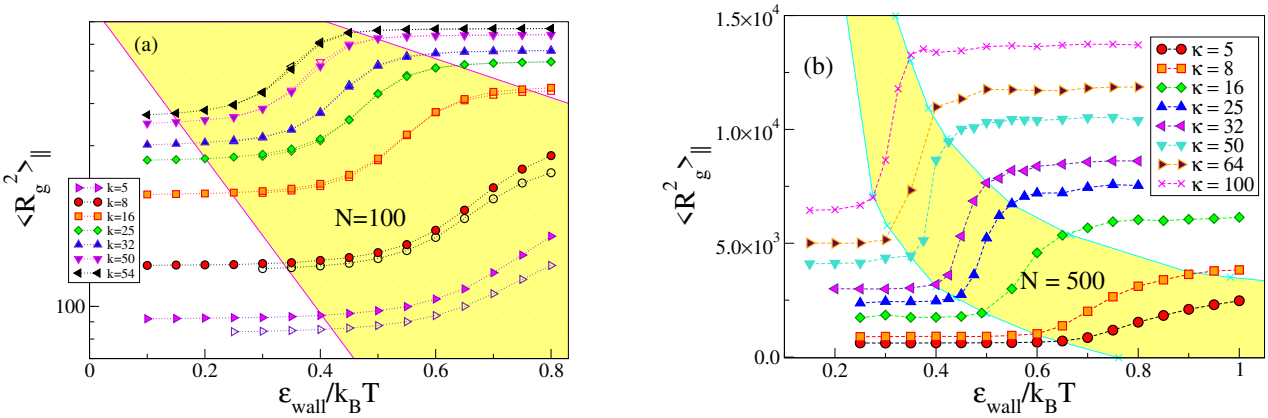

FIG. 11: Plot of $\langle R_{g||}^2 \rangle$ vs. $\epsilon_{\rm wall}/k_BT$ for $N = 100$ (a) and for $N = 500$ (b) within a broad range of values for κ. In (a) both data with excluded volume (full symbols) and without it (open symbols) are included. The horizontal region of small $\epsilon_{\rm wall}/k_BT$ correspond to the $d = 3$ mushroom case. The region of gradual transition is shaded, and the horizontal plateaus on the right side (large $\epsilon_{\rm wall}/k_BT$, are only reached for large enough κ) correspond to the $d = 2$ strongly adsorbed chains.

In order to disentangle the effects due to EV (which causes ultimately the crossover of $C(n)$ to a power law, cf. Eq. (15)), and the effects due to adsorption-induced crossover of the decay length $\ell_p^{\rm eff}$ from κ to 2κ {cf. Eqs. (13), (14)}, it is useful to study $C(n)$ for chains where EV interactions are shut off (Fig. 10c). Restricting attention to the strongly adsorbed case ($\epsilon_{\rm wall} \geq 0.8$), we are always able to fit an exponential decay law to the data, but it significantly differs from Eqs. (13), (14)

$$C(n) = A\exp(-n\ell_b/\ell_p^{\rm eff}), \quad \text{large}\, n, \tag{45}$$

where A is slightly smaller than unity and $\ell_p^{\rm eff}/\ell_b$ slightly smaller than 2κ, if κ is not extremely large. Eq. (45) provides a smooth crossover from Eq. (13) to Eq. (14) in the transition region

of the adsorption transition, and consequently there must occur a gradual transition between the description of $\langle R_g^2\rangle_{||}$ in the $d = 3$ case {Eq. (19)} and the $d = 2$ case {Eq. (21)}. This gradual transition is experienced when $\epsilon_{\rm wall}$ increases (Fig. (11). Note that data for $\langle R_{g||}^2\rangle$ where EV is switched off always fall somewhat below the data where EV is included, and as expected, for the quasi-two-dimensional strongly adsorbed chains, this effect of EV is more important. Data similar to Fig. 11 for $N = 250$ have already been given in our preliminary publication [62]; the smaller N the broader is the region of $\epsilon_{\rm wall}/k_BT$ over which the transition to the strongly adsorbed state is rounded; at the same time, the effect of EV becomes less important, since L then is no longer very much larger than $\ell_p^{\rm eff}$.

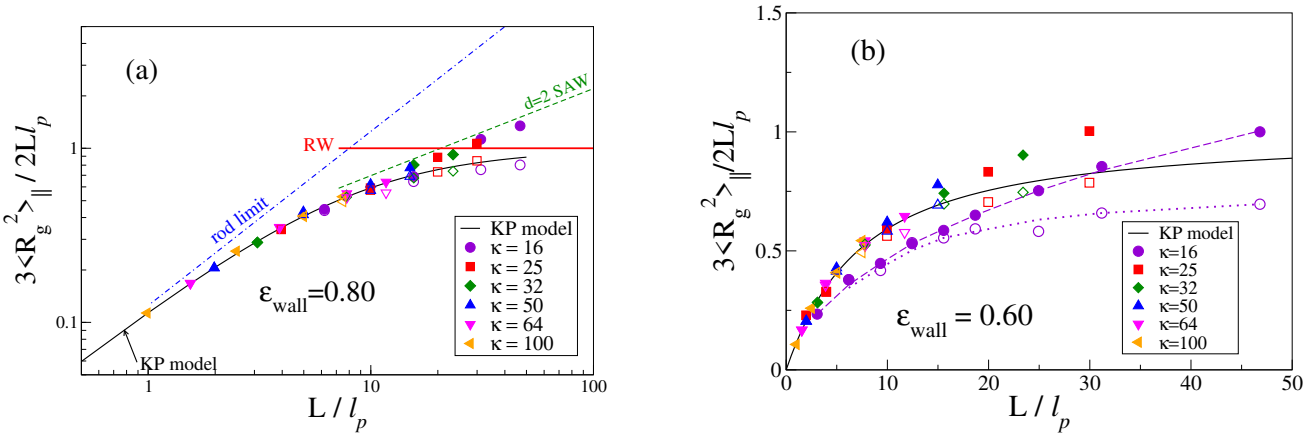

FIG. 12: Plot of $3\langle R_{g||}^2\rangle/(2\ell_pL)$ vs. L/ℓ_p for $\kappa = 16, 25, 32$ and 50, as indicated, and two choices of $\epsilon_{\rm wall} = 0.8$ (a) and 0.6 (b). Both data with (full symbols) and without (open symbols) excluded volume interactions are included. Part (a) presents the same data as log-log plot, to indicate the asymptotic behavior for large L/ℓ_p: the random walk limit (horizontal plateau) is approached by the KP model, while the actual data with EV approach the $d = 2$ self-avoiding walks (SAW) limit. Broken curves in part (b) are guides to the eye only.

As a consequence of this gradual change in the properties of the chains with increasing strength of the adsorption potential, which also depends very sensitively both on the intrinsic chain stiffness (as measured in our model by the parameter κ) and the chain length, great care is needed when Eqs. (20), (21) are used to analyze experimental data on adsorbed chains. Often AFM data on adsorbed DNA with contour lengths L in the same range as ℓ_p are analyzed (sometimes with the intention to identify subtle effects due to differences in the base pair sequences of ds DNA from various sources). The present results raise doubts on the validity of such analyses. As an example, we plot our data for two choices of $\epsilon_{\rm wall}$ in the adsorbed regime, Fig.12, in the form suggested by Eq. (21), namely $3\langle R_g^2\rangle_{||}/(2\ell_pL)$ is plotted vs. L/ℓ_p (note that in our model $L/\ell_p = (N-1)/\kappa$ and $\ell_pL = \kappa(N-1)\langle\ell_b^2\rangle$). For $L/\ell_p \le 5$ the data follow the KP model, but in this regime the deviations from the rod limit (which has no information on the actual value of ℓ_p whatsoever!) are minor. For $L/\ell_p > 5$ we see that part of the data falls above the KP result and part below it. The enhancement of $\langle R_g^2\rangle_{||}$ relative to the KP result can be attributed to excluded volume, and consequently these deviations become the more important the larger L/ℓ_p is. The deviations when $\langle R_g^2\rangle_{||}$ falls below the KP result, on the other hand, are due to the fact that then the gradual crossover of $\ell_p^{\rm eff}$ from ℓ_p to $2\ell_p$ has not been completed.

This problem becomes more important the smaller κ is, of course, since then the proximity of the adsorption transition matters. Therefore in Fig. 12b the data for $\kappa = 16$ without EV (dotted curve) fall distinctly below the KP prediction (full line). With EV, a crossover to the $d = 2$ SAW is observed but the prefactor of the power law is smaller than for $d = 2$ SAW in part (a). For $\kappa = 16$ indeed $\epsilon_{\rm wall}^{\rm cr} = 0.53$ is close to the studied value $\epsilon_{\rm wall} = 0.60$, and the strong depression of these

data away from the KP results is easily explained because the data still fall in the regime of only weekly adsorbed chains. Note that it may happen that data fall precisely on top of the KP curve due to a lucky cancellation of corrections: this happens for the data for $\epsilon_{\rm wall} = 0.6$ and $\kappa = 16$ near $L/\ell_p \approx 31$: if EV is switched off, the data fall below the KP curve. In contrast, for $\kappa = 50$ the data including EV are distinctly larger than the KP result.

To elucidate the crossover to the self-avoiding walk limit for large L/ℓ_p, we note from Huang et al. [60] that $\langle R^2(L)\rangle = 0.74 L^{3/2} (\ell_p^{\rm eff})^{1/2}$ where $\ell_p^{\rm eff}$ in strictly $d = 2$ dimensions is $\ell_p^{\rm eff} = 2\ell_p$. Combining this with the result for the universal ratio [90]

$$\langle R_g^2\rangle / \langle R^2\rangle = 0.14026 \pm 0.00011 \tag{46}$$

we predict that $\langle R_g^2\rangle = 0.1468 L^{3/2} \ell_p^{1/2}$ in $d = 2$, and this yields the straight line included in the log-log plot (Fig. 12a) which indeed is compatible with our data.

Already in our preliminary work [62], we have shown that in the nonadsorbed phase, for $\epsilon_{\rm wall} \ll \epsilon_{\rm wall}^{\rm cr}$, the linear dimension $\langle R_g^2\rangle_{||}$ is compatible with the result one predicts from the KP result {Eq. (19)} for $d = 3$ in the bulk (i.e., $\langle R_g^2\rangle_{||} = \frac{2}{3}\langle R_g^2\rangle_{d=3}$). We do not follow up on this here, because the coil conformations are not strictly isotropic (for very small $\epsilon_{\rm wall}$ we find that $\langle R_{gz}^2\rangle$ slightly exceeds $\frac{1}{2}\langle R_g^2\rangle_\perp$ while $\langle R_{gz}^2\rangle$ slightly but systematically decreases (and $\langle R_g^2\rangle_{||}$ slightly increases) with increasing $\epsilon_{\rm wall}$; so these data do not provide a very accurate test of Eq. (19). Actually, this slight dependence of the radii in the nonadsorbed phase is also responsible for the gradual decrease of the ratio $\langle R_g^2\rangle_\perp / \langle R_g^2\rangle_{||}$ for medium values of N, long before ϵ_{wall} has reached ϵ_{wall}^{cr}, see e.g., Fig. 4c, 4d, 5a.

VI. CONCLUSION

Using large-scale Molecular Dynamics simulation of a coarse-grained model for semiflexible macromolecules, the effect of chain stiffness on the adsorption transition and the structural properties of adsorbed chains have been clarified. The adsorbing impenetrable perfectly planar walls were described by the wall potential, Eq. (32), which has a strength $\epsilon_{\rm wall}$ and a minimum at a short distance from the surface. The semiflexible macromolecules were described as a chain of beads of diameter $\sigma(= 1)$ connected by (anharmonic) springs (the distances ℓ_b between neighboring beads being also about unity) and stiffness was controlled by a potential {Eq. (28)} of strength κ. For $\kappa \leq 1$ this model describes fully flexible chains, but for $\kappa > 2$ the chains are semiflexible, with persistence length (computable via Eq. (29) in $d = 3$ dimensions) $\ell_p/\ell_b = \kappa/k_BT$ $(= \kappa$, since $k_BT = 1$ throughout). The "chain length" (number of monomer units) N (and hence the contour length $L = (N-1)\ell_b$) was varied from 50 to 750, the stiffness κ from 5 to 100, and simulations were carried out also for the case where the excluded volume (EV) interaction between non-neighboring beads along the chain were shut off. In this case, our model constitutes a discretization of the Kratky-Porod (KP) wormlike chain model, to which it must reduce in the limit where N as well as ℓ_p/ℓ_b, are very large. Thus, our simulations are suited to clearly identify the conditions under which EV matters for semiflexible polymers.

Varying κ and using suitable extrapolations to the limit $N \to \infty$ (only in this limit the adsorption transition is a well-defined phase transition in the sense of statistical thermodynamics) we verify Semenov's [52] prediction for the variation of the location of the transition with chain stiffness, $\epsilon_{wall}^{\rm cr} \propto \ell_p^{-1/3}$. We also verify the expectation, that strongly adsorbed very stiff chains ($\kappa \gg 1$) behave like a KP model in $d = 2$ dimensions, with an effective decay length of orientational correlations $\ell_p^{\rm eff} = 2\ell_p$, i.e., twice as large as in $d = 3$ dimensions. However, we also show that near the adsorption transition the change of $\ell_p^{\rm eff}$ from ℓ_p to $2\ell_p$, takes place rather gradually, and there exists a region

of weak adsorption where the behavior of the chain is in many aspects "in between" $d = 2$ and $d = 3$ dimensions, e.g. orientational correlations (in the absence of EV) decay with distance s as $A\exp(-s/\ell_p^{\rm eff})$, with $A < 1$ and $\ell_p < \ell_p^{\rm eff} < 2\ell_p$. The extent $\Delta\epsilon_{\rm wall}$ of this region depends both on N and ℓ_p, however. This crossover has the effect that parallel linear dimensions $\langle R_g^2\rangle_{||}$ of the chains are less than the KP predictions while EV leads to deviations from KP predictions in the opposite direction (since in $d = 2$, where chain intersection is strictly forbidden, $\langle R_g^2\rangle_{||} \propto L^{3/2}\ell_p^{1/2}$ for $L \gg \ell_p$ rather than the KP prediction $\langle R_g^2\rangle_{||} \propto L\ell_p$, cf. Fig. 12a. As a consequence, we conclude that the interpretation of the variation of $\langle R^2\rangle$ and $\langle R_g^2\rangle$ with L is a very subtle problem for adsorbed chains, and the appropriateness of the KP predictions should be carefully examined.

A very interesting problem concerns the residual three-dimensional character of adsorbed chains, even in the strongly adsorbed case, the monomers are not confined strictly to the preferred plane $z = z_{\rm min}$, but make excursions above and below it (Fig. 2a). These excursions exhibit an obvious short-range correlation, over the length scale of Odijk's [54] deflection length. However, surprisingly both the adsorption order parameter f and the orientational order parameter η show a pronounced variation with $1/N$ as $N \to \infty$ in the regime of strong adsorption (cf. Figs. 7, 8), for very long chains the order being significantly more perfect (Fig. 9) than for shorter ones. This fact implies that small-amplitude long wavelength excitations around the contour of an adsorbed chain (which are the more suppressed the shorter a chain is) must play a decisive role in helping to stabilize a long chain in the strongly adsorbed state. It remains an exciting problem for the future to clarify the nature of this phenomenon in more detail, as well as the dependence of the perpendicular linear dimension $\langle R_{gz}^2\rangle$ and the deviation of η from parallel bond orientation (Fig. 8) on chain stiffness. Thus, we have found that the behavior of semiflexible adsorbed polymers is very rich, and from the theoretical point of view, not yet fully understood. We hope that the present work will motivate experiments as well as theoretical studies to provide a full understanding. Acknowledgment: One of us (A.M.) is grateful to the Alexander-von-Humboldt foundation for financial support and also thanks the COST action No. CA17139, supported by COST (European Cooperation in Science and Technology [91]) and its Bulgarian partner FNI/MON under KOST-11.

---

[1] C.J. Fleer, M.A. Cohen-Stuart, J.M.M. Scheutjens, T. Cosgrove, and B. Vincent, *Polymers at Interfaces* (Chapman & Hall, London, 1993)
[2] E. Eisenriegler, *Polymers Near Surfaces* (World Scientific, Singapore, 1993)
[3] P. G. de Gennes, Adv. Colloid Interfaces Sci. **27**, 189 (1987)
[4] R.R. Netz and D. Andelman, Phys. Rep. **380**, 1 (2003)
[5] J. Baschnagel, H. Meyer, J. Wittmer, I. Kulić, H. Mohrbach, F. Ziebert, G.M. Nam, N.-K. Lee, and A. Johner, Polymers **8**, 286 (2016)
[6] B. Liu, S. Salgado, V. Maheshwari, and J. Liu, Current Opinion Colloid. & Interface Sci. **26**, 41 (2016)
[7] R. Sinha, H.L. Frisch, and F.R. Eirich, J. Chem. Phys. **57**, 584 (1953)
[8] R. J. Rubin, J. Chem. Phys. **43**, 2392 (1965)
[9] P.G. de Gennes, J. Phys. (Paris) **37**, 1445 (1976)
[10] Y. Lépine and A. Caillé, Can. J. Phys. **56**, 403 (1978)
[11] P.G. de Gennes, Macromolecules **14**, 1637 (1981)
[12] E. Eisenriegler, K. Kremer, and K. Binder, J. Chem. Phys. **77**, 6296 (1982)
[13] T. Kreer, S. Metzger, M. Müller, K. Binder, and J. Baschnagel, J. Chem. Phys. **120**, 4012 (2004)
[14] S. Bhattacharya, H.-P. Hsu, A. Milchev, V.G. Rostiashvili, and T.A. Vilgis, Macromolecules **41**,

2920 (2008)
[15] L.I. Klushin, A.A. Polotsky, H.-P. Hsu, D.A. Markelov, K. Binder, and A.M. Skvortsov, Phys. Rev. E**87**, 022604 (2013)
[16] A. Grosberg and A.R. Khokhlov, *Statistical Physics of Macromolecules* (AIP Press, New York, 1994)
[17] M. Rubinstein and R.H. Colby, *Polymer Physics* (Oxford University Press, New York, 2003)
[18] G.L. Brelsford and W.R. Krigbaum, *Liquid Crystallinity in Polymers: Principles and Fundamental Properties* (VCH Publishers, New York, 1983) p. 61.
[19] H.-P. Hsu, W. Paul, and K. Binder, Macromolecules **43**, 3094 (2010)
[20] W. Reisner, J.N. Pederson, and R.H. Austin, Rep. Progr. Phys. **75**, 106601 (2012)
[21] S. Fraden, *Observation, Prediction, and Simulation of Phase Transitions in Complex Fluids* (Kluwer Acad. Publ.; Dordrecht, 1995) p. 113.
[22] M. Hase and K. Yoshikawa, J. Chem. Phys. **124**, 104903 (2006)
[23] C.R. Safinya, I. Koltover, and J. Raedler, Current Opin. Colloids & Interface Sci. **3**, 69 (1998)
[24] B. Maier and J.O. Rädler, Phys. Rev. Lett. **82**, 1911 (1999)
[25] B. Maier and J.O. Rädler, Macromolecules **33**, 7185 (2000)
[26] A. Kato, E. Shindo, T. Sakaue, A. Tsuji, and K. Yoshikawa, Biophys. J. **97**, 1678 (2009)
[27] C. Rivetti, M. Guthold and C. Bustamante, J. Mol. Biol. **264**, 919 (1996)
[28] J. Moukhtar, E. Fontaine, C. Faivre-Moskalenko, and A. Arneodo, Phys. Rev. Lett. **98**, 178107 (2007)
[29] K. Rechendorff, G. Witz, J. Adamcik, and G. Dietler, J. Chem. Phys. **131**, 095103 (2009)
[30] N. Mücke, K. Klenin, R. Kirmse, M. Bussiek, H. Herrmann, M. Hafner and J. Langowski, PLoS ONE **4**, e7756 (2009)
[31] J. Moukhtar, C. Faivre-Moskalenko, P. Milani, B. Audit, C. Vaillant, E. Fontaine, F. Mongelard, G. Lavorel, Ph. St-Jean, F. Argoul, and A. Arnoedo, J. Phys. Chem. B **114**, 5125 (2010)
[32] D. Welch, M.P. Lettinga, M. Ripoll, Z. Dogic and G.A. Vliegenthart, Soft Matter **11**, 7507 (2015)
[33] N. Gunari, M. Schmidt, and A. Janshoff, Macromolecules **39**, 2219 (2006)
[34] M. Sahl, S. Muth, R. Branscheid, K. Fischer, and M. Schmidt, Macromolecules **45**, 5167 (2012)
[35] K. Binder, H.-J. Butt, G. Floudas, H. Frey, H.-P. Hsu, K. Landfester, U. Kolb, A. Kühnle, M. Maskos, K. Müllen, W. Paul, M. Schmidt, H.W. Spiess, and P. Virnau *From Single Molecules to Nanoscopically Structured Materials* (Springer, Cham 2014) p. 115.
[36] H.-P. Hsu, W. Paul and K. Binder, J. Phys. Chem. B**115**, 14116 (2011)
[37] L. Grebikova, S. Kozhuharov, P. Maroni, A. Mikhaylov, G. Dietler, A.D. Schlüter, and M. Ullner, Nanoscale **8**, 13496 (2016)
[38] S.S. Sheiko, B.S. Sumerlin, and K. Matyjaszewki, Progr. Polym. Sci. **33**, 759 (2008)
[39] H.-P. Hsu, W. Paul, K. Binder, Macromol. Theory Simul. **20**, 510 (2011)
[40] I.V. Mikhailov, A.A. Darinskii, E.B. Zhulina, O.V. Borisov, and F.A. Leermakers, Soft Matter **11**, 9367 (2015)
[41] F. Dutertre, K.-T. Bang, B. Loppinet, I. Choi, T.-L. Choi, and G. Fytas, Macromolecules **49**, 2731 (2016)
[42] F. Dutertre, K.-T. Bang, E. Vereroudakis, B. Loppinet, S. Yang, S.-Y. Kang, G. Fytas, and T.-L. Choi, Macromolecules **52**, 3342 (2019)
[43] D. Messmer, Chr. Böttcher, H. Yu, A. Halperin, K. Binder, M. Kröger, and A.D. Schlüter, ACS Nano **13**, 3466 (2019)
[44] K. Binder (ed.) *Monte Carlo and Molecular Dynamics Simulations in Polymer Science* (Oxford University Press, New York, 1995)
[45] T.M. Birshtein, E.B. Zhulina, and A.M. Skvortsov, Biopolmyers **18**, 1171 (1979)

[46] A.R. Khokhlov, F.F. Ternovsky, and E.A. Zheligovskaya, Macromol. Chem., Theory Simul. **2**, 151 (1993)
[47] H.-P. Hsu and K. Binder, Macromolecules **46**, 2496 (2013)
[48] A.R. Khokhlov and A.N. Semenov, Macromolecules **17**, 2678 (1984)
[49] P.J. Flory, *Statistical Mechanics of Chain Molecules* (Interscience, New York, 1969)
[50] O. Kratky and G. Porod, J. Colloid Sci. **4**, 35 (1949)
[51] A.C. Maggs, D.A. Huse, and S. Leibler, Europhys. Lett. **8**, 615 (1989)
[52] A.N. Semenov, Euro. Phys. J.E **9**, 353 (2002)
[53] M. Deng, Y. Jiang, H. Liang, and J.Z.Y. Chen, J. Chem. Phys. **133**, 034902 (2010)
[54] T. Odjik, Macromolecules **16**, 1340 (1983)
[55] H. Nakanishi, J. Phys. (Paris) **48**, 979 (1987)
[56] J. Moon and H. Nakanishi, Phys. Rev. A**44**, 6427 (1987)
[57] H.-P. Hsu, W. Paul, and K. Binder, EPL **92**, 28003 (2010)
[58] H.-P. Hsu, W. Paul, and K. Binder, EPL **95**, 68004 (2011)
[59] A. Huang, A. Bhattacharya, and K. Binder, J. Chem. Phys. **140**, 214902 (2014)
[60] A. Huang, A. Bhattacharya, and K. Binder, J. Chem. Phys. **143**, 243102 (2015)
[61] J. des Cloizeaux and G. Jannink, *Polymers in Solution: Their Modeling and Structure* (Clarendon Press, Oxford, 1990)
[62] A. Milchev and K. Binder, Phys. Rev. Lett. **123**, 128009 (2019)
[63] L. Schäfer, A. Ostendorf, and J. Hager, J. Phys. A: Math. Gen. **32**, 7875 (1999)
[64] H. Benoit and P. Doty, J. Phys. Chem. **57**, 958 (1953)
[65] J.D. Weeks, D. Chandler, and H.C. Andersen, J. Chem. Phys. **54**, 5237 (1971)
[66] G.S. Grest and K. Kremer, Phys. Rev. A**33**, 3628 (1986)
[67] S.A. Egorov, A. Milchev, and K. Binder, Phys. Rev. Lett. **116**, 187801 (2016)
[68] S.A. Egorov, A. Milchev, P. Virnau, and K. Binder, Soft Matter **12**, 4944 (2016)
[69] A. Milchev, S.A. Egorov, and A. Nikoubashman, J. Chem. Phys. **149**, 174909 (2018)
[70] A. Milchev, A. Nikoubashman, and K. Binder, Comput. Materials Sci. **166**, 230 (2019)
[71] J. Kierfeld, O. Niamploy, V-Sa-Yakanit, and. R. Lipowsky, Eur. Phys. J.E. **14**, 17 (2004)
[72] T.A. Kampmann, H.-H. Boltz, and J. Kierfeld, J. Chem. Phys. **139**, 034903 (2013)
[73] T.A. Kampmann and J. Kierfeld, J. Chem. Phys. **147**, 014901 (2017)
[74] S. Naderi and P. van der Schoot, J. Chem. Phys. **141**, 124901 (2014)
[75] B. de Braaf, M.O. Menegon, S. Paquai, and P. van Schoot, J. Chem. Phys. **147**, 244901 (2017)
[76] A.M. Skvortsov, L.I. Klushin, A.A. Polotsky, and K. Binder, EPL **104**, 18009 (2013)
[77] A. Milchev and K. Binder, EPL **106**, 58001 (2014)
[78] A. Milchev, S.A. Egorov, and K. Binder, Soft Matter **10**, 5974 (2014)
[79] A. Milchev, S.A. Egorov, and K. Binder, Soft Matter **13**, 1888 (2017)
[80] A. Milchev and K. Binder, Nanoletters **17**, 4924 (2017)
[81] M.P. Allen and D.J. Tildesley, *Computer Simulation of Liquids*, 2nd ed. (Oxford University Press, Oxford 2017)
[82] L. Andersen, C. Lorenz, and J. Travesset, J. Comput. Phys. **227**, 5342 (2008)
[83] J. Glaser, T.D. Nguyen, J.A. Anderson, P. Liu, F. Spiga, J.A. Millan, D.C. Morse and S.C. Glotzer, Comput. Phys. Commun. **192**, 197 (2015)
[84] A. Nikoubashman, A. Milchev, and K. Binder, J. Chem. Phys. **145**, 234903 (2006)
[85] K. Binder and D.W. Heermann, *Monte Carlo Simulation in Statistical Physics. An Introduction* (Springer, Berlin, 1988)
[86] P.C. Hohenberg and B.I. Halperin, Rev. Mod. Phys. **49**, 435 (1977)
[87] N.-K. Lee and A. Johner, Macromolecules **48**, 7681 (2015)
[88] C.-T. Lee and E. M. Terentjev, Phys. Rev. E **100**, 032501 (2019)

[89] J.Z.Y. Chen, Progr. Polym. Sci. **34**, 3 (2016)
[90] A.D. Sokal, in Ref. [43], Chapter 2
[91] See http://www.cost.eu and https://www.fni.bg